Impact of reinfection with SARS-CoV-2 Omicron variants in previously infected hamsters

Nozomi Shiwa-Sudo,[a] Yusuke Sakai,[a] Naoko Iwata-Yoshikawa,[a] Shinji Watanabe,[b] Souichi Yamada,[c] Yudai Kuroda,[d] Tsukasa Yamamoto,[d] Masayuki Shirakura,[b] Seiichiro Fujisaki,[b] Kaya Miyazaki,[b] Hideka Miura,[b] Shiho Nagata,[b] Shuetsu Fukushi,[c] Ken Maeda,[d] Hideki Hasegawa,[b] Tadaki Suzuki,[a] Noriyo Nagata[a]#

[a]Department of Pathology, National Institute of Infectious Diseases, Tokyo, Japan.

[b]Research Center for Influenza and Respiratory Viruses, National Institute of Infectious Diseases, Tokyo, Japan.

[c]Department of Virology I, National Institute of Infectious Diseases, Tokyo, Japan.

[d]Department of Veterinary Science, National Institute of Infectious Diseases, Tokyo, Japan.

Running Head: Reinfection of SARS-CoV-2 variant in a hamster model

#Address correspondence to Noriyo Nagata, nnagata@niid.go.jp

Word counts for the abstract 241

Word counts for the importance 138

Word counts for the text 4997

ABSTRACT

The diversity of SARS-CoV-2 mutations raises the possibility of reinfection of individuals previously infected with earlier variants, and this risk is further increased by the emergence of the B.1.1.529 Omicron variant. In this study, we used an *in vivo*, hamster infection model to assess the potential for individuals previously infected with SARS-CoV-2 to be reinfected with Omicron variant and we also investigated the pathology associated with such infections. Initially, Syrian hamsters were inoculated with a lineage A, B.1.1.7, B.1.351, B.1.617.2 or a subvariant of Omicron, BA.1 strain and then reinfected with the BA.1 strain 5 weeks later. Subsequently, the impact of reinfection with Omicron subvariants (BA.1 and BA.2) in individuals previously infected with the BA.1 strain was examined. Although viral infection and replication were suppressed in both the upper and lower airways, following reinfection, virus-associated RNA was detected in the airways of most hamsters. Viral replication was more strongly suppressed in the lower respiratory tract than in the upper respiratory tract. Consistent amino acid substitutions were observed in the upper respiratory tract of infected hamsters after primary infection with variant BA.1, whereas diverse mutations appeared in hamsters reinfected with the same variant. Histopathology showed no acute pneumonia or disease enhancement in any of the reinfection groups and, in addition, the expression of inflammatory cytokines and chemokines in the airways of reinfected animals was only mildly elevated. These findings are important for understanding the risk of reinfection with new variants of SARS-CoV-2.

IMPORTANCE

The emergence of SARS-CoV-2 variants and the widespread use of COVID-19 vaccines has resulted in individual differences in immune status against SARS-CoV-2. A decay in immunity over time and the emergence of variants that partially evade the immune response can also lead to reinfection. In this study, we demonstrated that, in hamsters, immunity acquired following primary infection with previous SARS-CoV-2 variants was effective in preventing the onset of pneumonia after reinfection with the Omicron variant. However, viral infection and multiplication in the upper respiratory tract were still observed after reinfection. We also showed that more diverse nonsynonymous mutations appeared in the upper respiratory tract of reinfected hamsters that had acquired immunity from primary infection. This hamster model reveals the within-host evolution of SARS-CoV-2 and its pathology after reinfection, and provides important information for countermeasures against diversifying SARS-CoV-2 variants.

INTRODUCTION

After the emergence of the severe acute respiratory syndrome coronavirus 2 (SARS-CoV-2), at the end of 2019, various Variants of Concern (VOC) emerged, including the B.1.1.7 (Alpha), B.1.351 (Beta) and B.1.617.2 (Delta) strains, allowing COVID-19 infection to spread and persist worldwide (1). At the end of November 2021, the World Health Organization designated a variant of SARS-CoV-2, B.1.1.529, as a VOC (2). The B.1.1.529, Omicron variant, has 30 amino acid substitutions, three deletions, and one insertion site in the spike region compared with the ancestral, Wuhan, SARS-CoV-2 strain, including 15 mutations in the receptor binding region (3). The emergence of Omicron strains with high transmission capacity has changed the infection risk situation for the current COVID-19 pandemic (3, 4). Although several studies indicate that Omicron variants cause less severe disease than the Delta variant (5), it is clear that an individual infected with an earlier VOC or Omicron strain is still at risk of reinfection with the next variant, including Omicron subvariant (6). In addition, infection with Omicron is considered primarily as an upper respiratory tract infection. This differs from the pathophysiology associated with the earlier VOC, which tended to cause lower respiratory tract infection (7-10). Thus, there is increasing concern about the efficacy of immunity of previously infected individuals against the new variants and impact of immunopathology due to reinfection of SARS-CoV-2 (11, 12).

The Syrian hamster is more susceptible to SARS-CoV-2 than other animal species (13). Weight loss, clinical signs, pathology, and immune response can be used as indicators of viral infection in hamsters, making them a useful small animal model for development of vaccines and antiviral agents for COVID-19 (13-15). Several research groups have also used this animal model to investigate the phenotype of mutant viruses by testing for

changes in infectivity, infectiousness, and antigenicity (16, 17). Hansen et al used a hamster model to conduct reinfection experiments with a homologous, ancestor strain, WA1, and heterologous B.1.1.7 (Alpha) and B.1.351 (Beta) SARS-CoV-2 variants to determine the transmission through reinfection of asymptomatic individuals (18). Reinfection leads to SARS-CoV-2 replication in the upper respiratory tract with the potential for virus shedding, suggesting the risk of transmission through reinfected asymptomatic individuals. On the other hand, another group showed that prior infection with the WA1 strain prevented Delta variant transmission to naïve hamsters (19). In this study, therefore, we used a hamster model to i) evaluate the risk of reinfection with Omicron BA.1 strain, following infection with prior VOC strains, and ii) determine the risk of reinfection with Omicron subvariants in individuals first infected with the Omicron BA.1 strain.

RESULTS

Primary infection of hamsters with SARS-CoV-2 variants.

Five isolates of SARS-CoV-2 including the ancestor strain from lineage A, and four isolates of the VOC (B.1.1.7, B.1.351, B.1.617.2 and B.1.1.529; BA.1.18 [referred to as BA.1]; Table 1) were used for primary inoculation of Syrian hamsters as depicted in Figure 1A. Because hamsters are highly susceptible to SARS-CoV-2, primary infection was conducted by intranasal inoculation of a low dose of virus (1.0×10^3 $TCID_{50}$ in 8 µL of Dulbecco's Modified Eagle Medium (DMEM)), which reached the local upper respiratory tract, and induced seroconversion. Five weeks after primary infection, the lower respiratory tract of animals was then reinfected with a higher dose (1.0×10^4 $TCID_{50}$ in 50 µL) of virus. After the primary inoculation, animals infected with isolates from lineage A, B.1.1.7, and B.1.617.2 showed significantly lower weight gain rate than the mock-infection group

(DMEM in Figure 1B, n = 3–4) in the first week post-inoculation (p.i.) but showed no differences by four weeks p.i. (Figure 1B). At four weeks p.i., all animals, except those inoculated with the B.1.1.529; BA.1 strain, showed high antibody titers against the ancestor strain, lineage A and poor neutralizing activities against B.1.1.529; BA.1 strain (Figure 1C). The B.1.1.529; BA.1 strain-inoculated animals had neutralizing antibodies (1:64) against the homologous strain, but no neutralizing activities against the ancestor strain (detection limit was 1:16). Sera were also used in a multiple assay for antibodies that block the binding of human ACE2 to the spike proteins from variants of SARS-CoV-2 (Figure 1D). Lower inhibition activity against the spike from the B.1.1.529; BA.1 variant was seen in the sera from the A-, B.1.1.7-, and B.1.617.2-inoculated animals than in the sera from the B.1.351- and B.1.1.529 especially when used 1:100 diluted sera; BA.1-infected animals. Significantly, poor inhibition activity against the earlier VOC spike forms was observed in sera from the B.1.1.529; BA.1-infected animals.

Reinfection of hamsters with an Omicron variant.

Five weeks after the primary inoculations, the B.1.1.529; BA.1 strain was inoculated into all animals. No obvious respiratory illness was seen in any reinfected animals in the three days after the second inoculation. The homologous reinfected hamsters (BA.1-BA1 group in Figure 2A) showed transient body weight loss at 1 day post second infection unlike the mock infected- and primary infected-animals (DMEM group and DMEM-BA.1 group, respectively) by day 3 (Figure 2A). Three days after the second inoculation, all animals were euthanized, under overdose anesthesia, and blood, nasal wash fluid, and lung samples were obtained. The reinfected groups (A-BA.1 and B.1.1.7-BA.1 groups) showed significantly higher lung weight/body weight ratios at 3 days p.i. (Figure 2B). Infectious

virus was detected in the respiratory samples of some of the primary infected hamsters (DMEM-BA.1 group, one of four in the nasal wash fluid; three of four in the lung homogenate), but no infectious virus was recovered from any of the reinfected animals (Figure 2C; detection limit was $10^{1.5}$ $TCID_{50}$/mL). Interestingly, high viral RNA levels were detected in the nasal wash fluid from almost all animals, even though infectious virus was not isolated from these animals (Figure 2D upper panels). By contrast, no virus-associated RNA was detected in the lungs of animals with prior homologous BA.1 infection (BA.1-BA.1 group), and much lower virus copy numbers of virus-related RNA were detected in the lungs of animals with prior heterologous SARS-CoV-2 infection compared with those in the lungs of animals of DMEM-BA.1 group (Figure 2D lower panels). Thus, both prior homologous and heterologous SARS-CoV-2 infection elicited lower immune protection in the upper respiratory tract than that in the lower respiratory tract in this animal model.

The full-genome sequence of each of the Omicron BA.1 variants recovered from the nasal wash fluid samples was determined (Supplementary Table 1). Nsp15 (ORF1b: K2340T) and ORF10 (ORF10: V30L) nonsynonymous mutations appeared in all four hamsters whose primary infection was with BA.1. (Figure 2E, left). Three of the four animals also harbored variants with one or two amino acid substitutions in ORF1a region (nsp1:G180E and/or nsp6:L260F). The same within-host variants could be observed in the animals from the DMEM-BA.1 group. However, in the animals with prior homologous BA.1 infection (BA.1-BA.1 group), nonsynonymous mutations were unevenly distributed among individuals with low or high frequency mutations in nonstructural genes (nsp6:L37F, nsp6:L260F, nsp9:T67A, nsp10:Q36R, nsp15:K289T) and structural genes (S: M1del and ORF10: V30L). Mutations with greater diversity were also detected from animals subjected to prior heterologous SARS-CoV-2 infection (Supplementary Table 1, Figure 2E, right).

Common nonsynonymous mutations were observed in the upper respiratory tract of BA.1-primary infected hamsters, but diverse mutations appeared in that of BA.1-reinfected hamsters.

Pathology in the respiratory tract after reinfection.

Histopathological changes in reinfected animals were determined. Three days after reinfection, pathological lesions consisted of mild to moderate rhinitis and focal broncho-interstitial pneumonia in the respiratory tract of the primary infection group (DMEM-BA.1 group, Figure 3A, second row). SARS-CoV-2 N antigen-positive cells were observed both in the respiratory and olfactory epithelium of the nasal cavity and in bronchiolar epithelium and alveolar epithelia of the lungs (Figure 3B).

In the homologous infection group (BA.1-BA.1), the lungs were hardly damaged by the primary infection and the onset of pneumonia, following reinfection, was prevented (Figure 3A-D). By contrast, the heterologous reinfection groups showed moderate lymphocyte infiltration in the respiratory area of nasal cavity in the absence of viral antigens, except in a few animals from the B.1.1.7-BA.1 group (two of four animals) and the B.1.617.2-BA.1 group (one of four animal); viral antigens were detected in the epithelia of these animals and marked lymphocytic infiltration was observed from the lamina propria into the epithelium with or without multilayering of respiratory epithelial cells (regeneration) in the nasal cavity (Supplementary Figure 1 and Figure 3A). The lungs from the heterologous reinfection groups showed small clusters of lymphocytes, plasma cells, and macrophages around the bronchioles and blood vessels in the absence of detectable viral antigens (Supplementary Figure 1, Figure 3A, B, and C). Bronchiolar regeneration was also observed in the reinfection groups. In particular, the epithelial regeneration was more

pronounced in the lungs of the A-BA.1 group than in the lungs of other groups, indicating the severe damage caused by the primary infection with the lineage A strain (Supplementary Figure 1). In the B.1.617.2-BA.1 group, lymphocyte and macrophage infiltration was predominantly seen around the bronchioles, as reflected in the lung tissue score (Figure 3D). Fibrin deposition in the lungs is one of the main histopathological features of COVID-19 related acute pneumonia (20, 21). Fibrin deposition was often observed in lungs of the primary infected animals but in very few of the reinfected animals (Figure 3E).

High levels of cytokines and chemokines, including CXCL10/IP-10 and IL-1β, were observed in the nasal wash fluid of the primary infection group (DMEM-BA.1), but these were lower in reinfected animals (Figure 3F). Neither primary nor secondary infections with the BA.1 strain induced cytokine and chemokine profiles typically associated with pneumonia. Exacerbated cytokine production due to reinfection was not observed in either the upper or lower respiratory tract. Taken together, these data suggest that viral replication after reinfection was more strongly suppressed in the lower respiratory tract than in the upper respiratory tract.

Experimental hamster infection with Omicron subvariants

Next, we evaluated the risk of reinfection with B.1.1.529, Omicron subvariants in hamsters first infected with the BA.1 strain. Hamsters were infected as above, using four isolates of the B.1.1.529 subvariants (BA.1, BA.1.1, BA.2 and BA.2.3; Table 1) were used for primary and/or secondary inoculation of Syrian hamsters as depicted in Figure 4A. After primary inoculation with the BA.1 strain, animals showed slightly lower weight gain rate than the control animals (n = 16) during the first week p.i. but no difference was evident by the

second week p.i. (Figure 4B). At four weeks p.i., all BA.1 strain-inoculated animals showed seroconversion (Figure 4C). Clear antigenic differentiation between the BA.1 and BA.2 subvariants was shown in the sera from hamsters. While no neutralizing activity against the BA.2 strain was detected by a neutralization assay (Figure 4C), an assay measuring antibodies that block the binding of human ACE2 to spike proteins suggested the BA.1-infected hamster sera had inhibition activities against the spike from Omicron subvariants (Figure 4D).

Five weeks after the primary inoculation, B.1.1.529 subvariants (n = 4 per subvariant) were inoculated into the animals. No obvious respiratory illness was seen in any of the animals in the three days following the second inoculation. Body weight graphs did not show any significant difference between the primary and the reinfection groups (Figure 4E). Only animals infected with the BA.2 variant showed a significant difference in the lung/body weight ratio between primary and reinfection groups (Figure 4F). Infectious virus was detected from the respiratory samples of most hamsters after primary infection, but very low or no infectious virus was detected in samples from the reinfected animals (Figure 4G). However, infectious virus was detected in the nasal wash of three of the four animals in the BA.1-BA.1 reinfection group and the lungs of one of the four animals in the BA.1-BA.2 reinfection group. Despite the absence of infectious virus, high copy numbers of virus-associated RNA were detected in nasal lavage fluid from both homologous and heterologous reinfected animals. By contrast, significantly lower copy numbers of virus-associated RNA were detected in the lungs of reinfected animals than in those of the primary infected group (Figure 5A). Thus, animals with prior infection with BA.1 showed low protection of the upper respiratory tract against reinfection with the subvariants.

The full-genome sequence of each of the B.1.1.529 subvariants recovered from the nasal

wash fluid samples was determined (Supplementary Table 2 and 3). As in the earlier infection study, nsp15 (ORF1b: K2340T) and ORF10 (ORF10: V30L) nonsynonymous mutations appeared in all animals whose primary infection was with BA.1. (Figure 5B). In reinfected animals, several mutations were detected in nonstructural and structural genes of the variants, though the mutations were unevenly distributed among the infection groups (Figure 5B). Interestingly, for three of the four infection groups fewer within-host variants were detected following primary infection than were detected following reinfection.

In animals from all primary infection groups, pathological lesions consisted of mild to moderate rhinitis and focal broncho-interstitial pneumonia in the respiratory tract associated with virus infection (Figure 6A-D). Animals in the reinfection groups showed very slight to moderate lymphocyte infiltrations in the nasal cavity in the presence or absence of viral antigen (Figure 6A-C). Some animals from the reinfection groups (BA.1-BA.1, one of four; BA.1-BA.1.1, two of four; BA.1-BA.2, two of four in each group) showed focal infiltrations with lymphocytes, plasma cells, and macrophages in the alveoli and around the blood vessels. In reinfected animals, lung pathology occurred even though viral antigen was detected in only one of the animals from the BA.1-BA.2 group (Figure 6A-D). Fibrin deposition was observed in the lungs of most animals after primary infection but in the lungs of very few reinfected animals (Figure 6E). High levels of CXCL10/IP-10 and IL-1β were observed in the nasal wash fluid and lungs of the primary infection groups, but the levels were lower in reinfection animals (Supplementary Figure 2). Thus, exacerbated cytokine production, due to reinfection, was not seen in either the upper or lower respiratory tract. These data suggest that despite the fact that some animals reinfected with subvariants are unable to mount a sufficient immune response against reinfection, especially in the upper respiratory tract, they are still able to eliminate these variants more

rapidly, in early phase, than occurs in naïve animals. In addition, there were no findings suggesting disease exacerbation.

DISCUSSION

Plasma from convalescent human cases and from individuals who had been vaccinated against SARS-CoV-2 exhibited marked reductions in neutralizing activity against Omicron than against the ancestral SARS-CoV-2 (22-26). Multiple lineages of the Omicron variants have emerged including BA.1, BA.2, BA.3, BA.4 and BA.5, with the dominant strain being replaced by an emerging variant (27). Initially, BA.1 was the most prolific sublineage detected worldwide; however, BA.2 is overtaking BA.1 as the dominant variant and now BA. 5 has replaced (27). In human cases, lower neutralizing antibody titers against the BA.4 and BA.5 subvariants than against the BA.1 and BA.2 subvariants suggest that the Omicron variant is continuing to evolve with increasing capacity for neutralization escape (28). Consequently, the monitoring of antigenic changes in new SARS-COV-2 variants that emerge should continue. Syrian hamster models are considered to be ideal for determining the antigenic differences of SARS-CoV-2 variants (29, 30) and, as in a previous study (30), our hamster model showed clear antigenic differentiation between the BA.1 and BA.2 subvariants. Female hamsters were selected for the infection model used in this study since they show better systemic and local antiviral antibody responses and more prolonged humoral immunity, than male hamsters, following SARS-CoV-2 infection (31).

Because the strength of the humoral immune response and the duration of neutralizing antibodies may correlate with disease severity, viral shedding from individuals with mild COVID-19 is a concern (32). In hamsters, primary infection induced immune responses

with disease-protective capacity against reinfection by homologous or heterologous Omicron subvariants. In this study, the induction of immunity and neutralizing antibodies, during upper respiratory tract infection, was not a sufficient at preventing proliferation in the upper respiratory tract of hamsters, following reinfection, as reported in previous studies (16, 18, 19). The presence of infectious virus in the upper respiratory tract of hamsters, despite a significant decrease in virus levels following reinfection, suggests that even asymptomatic individuals are capable of shedding infectious virus that can cause infection. On the other hand, it appears that the virus was efficiently cleared from the lower respiratory tract in reinfected animals. Neutralizing antibodies in the blood are believed to be effective in preventing reinfection of the lower respiratory tract (33).

The sequence of variants recovered from hamster nasal wash fluid after reinfection was greater than 99.99% identical to that of the virus used for reinfection. SARS-CoV-2 population in a host is not represented by a single dominant sequence, but rather consists of an ensemble of replicating viruses comprised of closely related sequences called quasispecies (34). Consequently, the alteration of functional genes (such as the S gene) is likely to generate SARS-CoV-2 quasispecies that are better adapted for infection and survival in a particular host (35). Interestingly, viral RNA recovered from nasal washes, from all eight hamsters in two, separate, primary BA.1 infection experiments, showed consistent amino acid substitutions at Nsp15 (ORF1b: K2340T) and ORF10 (ORF10: V30L). By contrast, this consistency was less observed in viral RNA recovered after homologous and heterologous reinfection of Omicron variants, with amino acid substitutions occurring in more diverse regions. Nsp 15 of SARS-CoV-2 functions as an endoribonuclease (36). Nsp15 and several other SARS-CoV-2 proteins inhibit primary

298 interferon production and interferon signaling and thus may interfere with the body's
299 defense against infection (36-38). Compared with SARS-CoV and other nidoviruses, the
300 Orf10 protein of SARS-CoV-2 is a unique 38 aa protein (39). However, the role of ORF10
301 is still unclear. Interestingly, the overexpression of ORF10, *in vitro*, markedly suppressed
302 the expression of type I interferon genes (40). In addition, the V30L amino acid substitution
303 in ORF10 correlates with disease severity in COVID-19 patients (41). The significance of
304 these mutations observed in the hamsters remains to be elucidated.
305
306 One concern regarding reinfection with the SARS-CoV-2 subtype is that an abnormal
307 immune response to the primary infection may exacerbate the secondary infection and
308 enhance immunopathology (42), as is seen, for example, in antibody-dependent
309 enhancement (ADE) breakthrough infections such as dengue fever (43). Feline infectious
310 peritonitis (FIP), a coronavirus infection in cats, causes classic ADE disease (44, 45); in
311 contrast to FIP, SARS-CoV-2 infections in humans primarily involve the respiratory tract
312 and other organs but not the reticuloendothelial system. It is clear that the primary target of
313 SARS-CoV-2 infection is alveolar epithelial cells, which are directly injured by the virus
314 (46). Since myeloid cells are not the primary target of infection, it is unlikely that vaccine-
315 derived, non-protective, coronavirus antibodies will cause ADE infection in human (47). In
316 addition, no cases of enhanced disease due to reinfection with Omicron have been reported
317 (48-50). CXCL10/IP-10 has a well-established role in the COVID-19-related cytokine
318 storm and is involved in the development of severe lung impairment (51). Elevated levels
319 of key inflammatory chemokines and cytokines, such as CXCL10/IP-10 and IL-1β, were
320 observed in nasal wash fluid and lung homogenate supernatant of hamsters during primary
321 infection, but not after the reinfection. In addition, reinfected hamsters showed no evidence

of the eosinophil-associated lung inflammation observed, previously, in infected mice (52). Thus we concluded that pathological and cytokine/chemokine analyses showed no evidence of disease progression after reinfection in our hamster model. However, as new SARS-CoV-2 variants emerge, their virulence could change and, hence, there is a need to actively monitor variants.

Overall, the hamster model demonstrated that immunity acquired during primary infection, with a previous SARS-CoV-2 variant or early Omicron sublineage, suppressed the development of pneumonia after reinfection with a subsequently emerged variant. However, infection and multiplication in the upper respiratory tract after reinfection were inevitable, suggesting the likelihood of virus excretion in asymptomatic hamsters. The virus population in the upper respiratory of reinfected hamsters was shown to be more diverse than that seen in hamsters after primary infection. In addition, differences were observed between the BA.1 strain and other subvariants, in the diversity of virus populations generated in infected hamsters, which may reflect alterations in virus infectivity and replication within specific hamsters. These findings could provide a better understanding of pathology after reinfection by new variants of SARS-CoV-2. In addition, the hamster model should provide insight into the within-host evolution of SARS-CoV-2 and provide important information for countermeasures aimed at diversifying SARS-CoV-2 mutant strains.

MATERIALS AND METHODS

Ethics.

All procedures involving cells and animals were conducted in a Biosafety Level (BSL) 3

laboratory. All animal experiments were approved by the Animal Care and Use Committee of the National Institute of Infectious Diseases in Japan (approval nos. 120108, 120142, and 121152), and all experimental animals were handled in BSL3 animal facilities according to the guidelines of this committee (approval nos. 19-53, 20-39, and 20-31). All animals were housed in a facility certified by the Japan Health Sciences Foundation.

Viruses and cells.

Viruses were isolated from anonymized clinical specimens (nasopharyngeal/nasal swabs or saliva) collected from individuals diagnosed with COVID-19 as part of the public health diagnostic activities conducted by National Institute of Infectious Diseases (53, 54). VeroE6/TMPRSS2 cells purchased from the Japanese Collection of Research Bioresources Cell Bank (JCRB1819, the National Institute of Biomedical Innovation, Health and Nutrition, Osaka, Japan) were used for viral isolation and viral titrations (53). Cells were cultured in DMEM, low glucose (Sigma-Aldrich, St. Louis, MO), containing 10% FBS, 50 IU/mL penicillin G, and 50 μg/mL streptomycin (10DMEM). Viral infectivity titers were expressed as $TCID_{50}$/mL in VeroE6/TMPRSS2 cells and were calculated according to the Behrens–Kärber method. Work with infectious SARS-CoV-2 was performed under BSL3 conditions.

Animal experiments.

Five-week-old female Syrian golden hamsters (SLC, Shizuoka, Japan) were used for animal experiments. After anesthesia, animals were inoculated intranasally with 1.0×10^3 $TCID_{50}$ (in 8 μL) of one of five isolates of SARS-CoV-2 including the ancestor strain from lineage A, and four isolates of the VOC (lineage B.1.1.7, B.1.351, B.1.617.2, and B.1.1.529 BA.1; Table 1) . All mock-infected hamsters were inoculated with DMEM containing 2% (v/v) FCS

containing 50 IU/mL penicillin G, and 50 μg/mL streptomycin (2DMEM). Body weight was measured daily for 3 days (n = 4 or 16 per group). Five weeks after their first inoculation, animals were then re-inoculated intranasally with 1.0×10^4 $TCID_{50}$ (50 μL) of four isolates of the B.1.1.529 subvariants (BA.1, BA.1.1, BA.2, BA.2.3; Table 1). Body weight was measured daily for 3 days (n = 3-4 per group), and animals were sacrificed at 3 days p.i. to analyze viral replication and disease pathology (n = 3-4 per group). The humane endpoint was defined as the appearance of clinically diagnostic signs of respiratory stress, including respiratory distress and more than 25% weight loss. Animals were euthanized under anesthesia with an overdose of isoflurane if severe disease symptoms or weight loss was observed.

RNA extraction and quantification of viral RNA genomes.

Total RNA from each lung homogenate and nasal wash was isolated using the Maxwell RSC Maxwell RSC Viral Total Nucleic Acid Purification Kit (Promega Corporation), following the manufacturer's suggested protocol, and quantified by NanoDrop (Thermo Fisher Scientific). The viral RNA copy number in the samples was estimated by real-time RT-PCR. Subgenomic viral RNA transcripts were also detected in N gene transcripts. The primer and probe sets are as follows: NIID_2019-nCOV_N_F2 (5'-AAATTTTGGGGACCAGGAAC-3'), NIID_2019-nCOV_N_R2 (5'-TGGCAGCTGTGTAGGTCAAC-3'), and NIID_2019-nCOV_N_P2 (5'-FAM-ATGTCGCGCATTGGCATGGA-BHQ-3') for targeting the viral RNA; and SARS2-LeaderF60 (5′-CGATCTCTTGTAGATCTGTTCTCT-3′), SARS2-N28354R (5′-TCTGAGGGTCCACCAAACGT-3′), and SARS2-N28313Fam (5′-FAM-TCAGCGAAATGCACCCCGCA-TAMRA-3′) for targeting the subgenomic RNA. The reaction mixtures were incubated at 50°C for 30 min, followed by incubation at 95°C for 15

min, and thermal cycling, which consisted of 40 cycles of denaturation at 94°C for 15 s, and annealing and extension at 60°C for 60 s. This assay was performed on a LightCycler 480 (Roche, Basel, Switzerland).

SARS-CoV-2 neutralizing assay

Blood was obtained from each hamster under anesthesia (55) and when euthanized. Sera were then obtained by centrifugation and were inactivated by incubation at 56°C for 30 min. Aliquots (100 $TCID_{50}$/well) of SARS-CoV-2 were incubated at 37°C for 1 h in the presence or absence of hamster serum (serially diluted two-fold), and then added to confluent VeroE6/TMPRSS2 cell cultures in 96-well microtiter plates. Samples were examined for viral cytopathic effects on Day 5, and the neutralizing antibody titers were determined as the reciprocal of the highest dilution at which no CPEs were observed. The lowest and highest serum dilutions tested were 1:16 and 1:2048, respectively.

ACE2 binding inhibition electrochemiluminescence immunoassay

A multiple assay for neutralizing antibodies to spike antigens from variants of SARS-CoV-2 using the V-PLEX SARS-CoV-2 (ACE2) kits (K15570U and K15586U, Meso Scale Discovery) was used. 1:10 and 1:100 diluted sera were used for the assay. The assay samples were read on a high-performance electrochemiluminescence immunoassay instrument, MESO QuickPlex SQ 120 (Meso Scale Discovery), as described by the manufacturer.

Detection of inflammatory cytokines and chemokines

Homogenized lung tissue samples (10% w/v) and nasal wash samples were diluted 1:1 in cell extraction buffer (10 mM Tris, pH 7.4, 100 mM NaCl, 1 mM EDTA, 1 mM EGTA, 1 mM

NaF, 20 mM $Na_4P_2O_7$, 2 mM Na_3VO_4, 1% Triton X-100, 10% glycerol, 0.1% SDS, and 0.5% deoxycholate (BioSource International, Camarillo, CA)), incubated for 10 min on ice with vortexing, irradiated for 10 min with UV-C light to inactivate infectious virus, and tested in the BSL2 laboratory. Cytokine and chemokine levels were measured with a commercial rat cytokine/chemokine magnetic bead panel 96-well plate assay kit (Milliplex MAP kit, Merck Millipore), which detects 5 cytokines and chemokines including IP-10/CXCL10, IL-1α, IL-1β, IL-10, and VEGF (56). The assay samples were read on a Luminex 200 instrument with xPONENT software (Merck Millipore), as described by the manufacturer.

Histopathology and immunohistochemistry

The lungs and head including nasal cavity and brain were harvested and fixed in 10% phosphate-buffered formalin. Fixed tissues were routinely embedded in paraffin, sectioned, and stained with hematoxylin and eosin (H&E). For immunohistochemistry, antigen retrieval of the formalin-fixed tissue sections was performed by autoclaving at 121°C for 10 min in retrieval solution at pH 6.0 (Nichirei, Tokyo, Japan). SARS-CoV-2 antigens were detected using a polymer-based detection system (Nichirei-Histofine Simple stain MAX PO; Nichirei Biosciences, Inc., Tokyo, Japan), and an in-house rabbit anti-SARS-CoV-2 N antibody was used as the primary antibody. Nuclei were counterstained with hematoxylin for 10 s.

Histopathology scores were determined based on the percentage of lesion area including inflammation, hemorrhage and edema, as determined by HE staining in each group by using the following scoring system: 0, no lesion; 1, focal lesion within 30% or less total area; 2, diffuse lesion involving 30–70% total area; 3, diffuse lesion involving more than 70% total area. Scores were also determined based on the percentage of virus antigen-

positive cells, as determined by immunohistochemistry in each group by using the following scoring system: 0, no antigen-positive cells; 1, antigen-positive cells were occasionally observed in each cut sections (1–3 antigen-positive areas per section were observed in the high magnification); 2, scattered positive cells were observed (4–9 antigen-positive areas per section were observed in the high magnification); 3, many positive cells were diffusely and widely observed (more than 10 antigen-positive areas per section were observed in the low magnification). Mean scores from all lung sections (four lung sections/animal) in each animal were calculated. Dots in figure indicate mean scores in each animal.

Next generation sequencing analysis for comparison of SARS-CoV-2 mutations

To identify major population of virus in respiratory tract of hamsters after reinfection, a next generation sequencer was used to obtain the entire length of the viral genome. The sequences obtained from the samples were compared with those of the inoculated viruses. The viral RNAs were extracted from the homogenized lung tissue samples (10% w/v) and nasal wash samples using the Maxwell® RSC Viral Total Nucleic Acid Purification Kit (Promega, Madison, WI). The whole genomes of SARS-CoV-2 used in this research were amplified using a modified ARTIC protocol with several primers replaced or added (57, 58). The viral cDNAs were synthesized from extracted RNA using the Luna Script RT Super Mix Kit (New England BioLabs, Ipswich, MA), followed by DNA amplification by multiplex PCR in two separated primer pools using ARTIC-N5 primers (59, 60) and Q5 Hot Start DNA polymerase (New England BioLabs). The DNA libraries for Illumina NGS were prepared from pooled amplicons using the QIAseq FX DNA Library Kit (QIAGEN) and analyzed using the iSeq 100 and MiSeq (Illumina). The obtained reads were analyzed

by the CLC Genomics Workbench (version 21, QIAGEN) with the Wuhan/Hu-1/2019 sequence (GenBank accession number MN908947) as a reference. The sequence data have been deposited in the DNA Data Bank of Japan (DDBJ) Sequence Read Archive, under submission (BioProject Accession: PRJDB14262; BioSample accessions: SAMD00523210-SAMD0052326). In the reinfection experiment, the frequencies of gene mutations were calculated with each protein. The average depth of aligned reads was 3132. In the co-infection experiment, the ratio of Delta and BA.1 was calculated as the percentages based on the 10 regions where these two viruses can be distinguished. The nucleotide numbers of these 10 regions are: 2832, 8393, 11537, 21618, 22673-22674, 23048, 23063, 23604, 26530, and 28311 of the Wuhan/Hu-1/2019 genome, which correspond to amino acids 856, 2710, 3758 in ORF1a, 19, 371, 496, 501, 681 in the spike protein, 3 in the M protein, and 13 in the N protein, respectively. The ratio of BA.1 and BA.2 was also analyzed based on the 10 regions where these two strains could be identified. The nucleotide numbers in these 10 regions are: 2832, 8393, 11537, 21618, 22204-22205, 22673-22674, 22786, 22898, 23048, and 29510 in the Wuhan/Hu-1/2019 genome, which correspond to amino acids 856, 2710, 3758 in ORF1a, 19, 214, 371, 408, 446, 496 in the spike protein, and 13 in the N protein, respectively. The average depth of aligned reads was 3132. Each read depth at the 20 regions used to calculate the ratios was more than 200.

Statistical analysis.

All data are expressed as the mean and standard error of the mean, except for neutralizing antibodies (Geometric mean titers with 95% confidence interval, GMT+95%Cl). Statistical analyses were performed using GraphPad Prism 9 software (GraphPad Software, La Jolla,

CA). Intergroup comparisons were performed using nonparametric analysis. A P value < 0.05 was considered statistically significant.

ACKNOWLEDGMENTS

We thank Dr Shutoku Matsuyama and Dr Makoto Takeda (National Institute of Infectious Disease) for providing SARS-CoV-2 isolates. We are grateful to Midori Ozaki, Takiko Yoshida, and Dai Izawa for their technical assistance and our colleagues at the Institute for helpful discussions. We thank the members of the Management Department of Biosafety and Laboratory Animals for support with the BSL3 facility.

This work was supported by the Grant-in-Aid for Scientific Research from the Ministry of Education, Culture, Sports, Science, and Technology in Japan (21K20767 to NS-S; 20K21666 to NN) and the Japan Agency for Medical Research and Development grants (JP21fk0108615 to KM and NN; JP21nf0101626 to HH; JP21wm0125008 to TS).

REFERENCES

1. **World_Health_Organization.** WHO coronavirus disease (COVID-19) dashboard, *on* World Health Organization. https://covid19.who.int. Accessed 15, Aug.
2. **World_Health_Organization.** 26 November 2021 2021. Classification of Omicron (B.1.1.529): SARS-CoV-2 Variant of Concern, *on* World Health Organization. https://www.who.int/news/item/26-11-2021-classification-of-omicron-(b.1.1.529)-sars-cov-2-variant-of-concern. Accessed May 29.
3. **Viana R, Moyo S, Amoako DG, Tegally H, Scheepers C, Althaus CL, Anyaneji UJ, Bester PA, Boni MF, Chand M, Choga WT, Colquhoun R, Davids M,**

Deforche K, Doolabh D, du Plessis L, Engelbrecht S, Everatt J, Giandhari J, Giovanetti M, Hardie D, Hill V, Hsiao N-Y, Iranzadeh A, Ismail A, Joseph C, Joseph R, Koopile L, Kosakovsky Pond SL, Kraemer MUG, Kuate-Lere L, Laguda-Akingba O, Lesetedi-Mafoko O, Lessells RJ, Lockman S, Lucaci AG, Maharaj A, Mahlangu B, Maponga T, Mahlakwane K, Makatini Z, Marais G, Maruapula D, Masupu K, Matshaba M, Mayaphi S, Mbhele N, Mbulawa MB, Mendes A, Mlisana K, et al. 2022. Rapid epidemic expansion of the SARS-CoV-2 Omicron variant in southern Africa. Nature **603:**679-686.

4. **Karim SSA, Karim QA.** 2021. Omicron SARS-CoV-2 variant: a new chapter in the COVID-19 pandemic. The Lancet **398:**2126-2128.

5. **Wolter N, Jassat W, Walaza S, Welch R, Moultrie H, Groome M, Amoako DG, Everatt J, Bhiman JN, Scheepers C, Tebeila N, Chiwandire N, du Plessis M, Govender N, Ismail A, Glass A, Mlisana K, Stevens W, Treurnicht FK, Makatini Z, Hsiao N-y, Parboosing R, Wadula J, Hussey H, Davies M-A, Boulle A, von Gottberg A, Cohen C.** 2022. Early assessment of the clinical severity of the SARS-CoV-2 omicron variant in South Africa: a data linkage study. The Lancet **399:**437-446.

6. **Pulliam JRC, Schalkwyk Cv, Govender N, Gottberg Av, Cohen C, Groome MJ, Dushoff J, Mlisana K, Moultrie H.** 2022. Increased risk of SARS-CoV-2 reinfection associated with emergence of Omicron in South Africa. Science **376:**eabn4947.

7. **Halfmann PJ, Iida S, Iwatsuki-Horimoto K, Maemura T, Kiso M, Scheaffer SM, Darling TL, Joshi A, Loeber S, Singh G, Foster SL, Ying B, Case JB, Chong Z, Whitener B, Moliva J, Floyd K, Ujie M, Nakajima N, Ito M, Wright**

R, Uraki R, Warang P, Gagne M, Li R, Sakai-Tagawa Y, Liu Y, Larson D, Osorio JE, Hernandez-Ortiz JP, Henry AR, Ciouderis K, Florek KR, Patel M, Odle A, Wong L-YR, Bateman AC, Wang Z, Edara V-V, Chong Z, Franks J, Jeevan T, Fabrizio T, DeBeauchamp J, Kercher L, Seiler P, Gonzalez-Reiche AS, Sordillo EM, Chang LA, van Bakel H, et al. 2022. SARS-CoV-2 Omicron virus causes attenuated disease in mice and hamsters. Nature.

8. **Iuliano AD, Brunkard JM, Boehmer TK, Peterson E, Adjei S, Binder AM, Cobb S, Graff P, Hidalgo P, Panaggio MJ, Rainey JJ, Rao P, Soetebier K, Wacaster S, Ai C, Gupta V, Molinari NM, Ritchey MD.** 2022. Trends in Disease Severity and Health Care Utilization During the Early Omicron Variant Period Compared with Previous SARS-CoV-2 High Transmission Periods - United States, December 2020-January 2022. MMWR Morb Mortal Wkly Rep **71:**146-152.

9. **Madhi SA, Kwatra G, Myers JE, Jassat W, Dhar N, Mukendi CK, Nana AJ, Blumberg L, Welch R, Ngorima-Mabhena N, Mutevedzi PC.** 2022. Population Immunity and Covid-19 Severity with Omicron Variant in South Africa. New England Journal of Medicine **386:**1314-1326.

10. **Fall A, Eldesouki RE, Sachithanandham J, Morris CP, Norton JM, Gaston DC, Forman M, Abdullah O, Gallagher N, Li M, Swanson NJ, Pekosz A, Klein EY, Mostafa HH.** 2022. The displacement of the SARS-CoV-2 variant Delta with Omicron: An investigation of hospital admissions and upper respiratory viral loads. eBioMedicine **79:**104008.

11. **Cromer D, Juno JA, Khoury D, Reynaldi A, Wheatley AK, Kent SJ, Davenport MP.** 2021. Prospects for durable immune control of SARS-CoV-2 and prevention of reinfection. Nature Reviews Immunology **21:**395-404.

12. **Wong L-YR, Perlman S.** 2022. Immune dysregulation and immunopathology induced by SARS-CoV-2 and related coronaviruses — are we our own worst enemy? Nature Reviews Immunology **22:**47-56.

13. **Rosenke K, Meade-White K, Letko M, Clancy C, Hansen F, Liu Y, Okumura A, Tang-Huau T-L, Li R, Saturday G, Feldmann F, Scott D, Wang Z, Munster V, Jarvis MA, Feldmann H.** 2020. Defining the Syrian hamster as a highly susceptible preclinical model for SARS-CoV-2 infection. Emerging Microbes & Infections **9:**2673-2684.

14. **Chan JF, Zhang AJ, Yuan S, Poon VK, Chan CC, Lee AC, Chan WM, Fan Z, Tsoi HW, Wen L, Liang R, Cao J, Chen Y, Tang K, Luo C, Cai JP, Kok KH, Chu H, Chan KH, Sridhar S, Chen Z, Chen H, To KK, Yuen KY.** 2020. Simulation of the clinical and pathological manifestations of Coronavirus Disease 2019 (COVID-19) in golden Syrian hamster model: implications for disease pathogenesis and transmissibility. Clin Infect Dis.

15. **Imai M, Iwatsuki-Horimoto K, Hatta M, Loeber S, Halfmann PJ, Nakajima N, Watanabe T, Ujie M, Takahashi K, Ito M, Yamada S, Fan S, Chiba S, Kuroda M, Guan L, Takada K, Armbrust T, Balogh A, Furusawa Y, Okuda M, Ueki H, Yasuhara A, Sakai-Tagawa Y, Lopes TJS, Kiso M, Yamayoshi S, Kinoshita N, Ohmagari N, Hattori SI, Takeda M, Mitsuya H, Krammer F, Suzuki T, Kawaoka Y.** 2020. Syrian hamsters as a small animal model for SARS-CoV-2 infection and countermeasure development. Proc Natl Acad Sci U S A **117:**16587-16595.

16. **Nunez IA, Lien CZ, Selvaraj P, Stauft CB, Liu S, Starost MF, Wang TT.** 2021. SARS-CoV-2 B.1.1.7 Infection of Syrian Hamster Does Not Cause More Severe

586 Disease, and Naturally Acquired Immunity Confers Protection. mSphere**:**e0050721.

587 17. **Abdelnabi R, Boudewijns R, Foo CS, Seldeslachts L, Sanchez-Felipe L, Zhang**
588 **X, Delang L, Maes P, Kaptein SJF, Weynand B, Vande Velde G, Neyts J,**
589 **Dallmeier K.** 2021. Comparing infectivity and virulence of emerging SARS-CoV-2
590 variants in Syrian hamsters. EBioMedicine **68:**103403.

591 18. **Hansen F, Meade-White K, Clancy C, Rosenke R, Okumura A, Hawman DW,**
592 **Feldmann F, Kaza B, Jarvis MA, Rosenke K, Feldmann H.** 2022. SARS-CoV-2
593 reinfection prevents acute respiratory disease in Syrian hamsters but not replication
594 in the upper respiratory tract. Cell Reports **38**.

595 19. **Halfmann PJ, Kuroda M, Armbrust T, Accola M, Valdez R, Kowalski-Dobson**
596 **T, Rehrauer W, Gordon A, Kawaoka Y.** 2022. Long-term, infection-acquired
597 immunity against the SARS-CoV-2 Delta variant in a hamster model. Cell Reports
598 **38**.

599 20. **Polak SB, Van Gool IC, Cohen D, von der Thüsen JH, van Paassen J.** 2020. A
600 systematic review of pathological findings in COVID-19: a pathophysiological
601 timeline and possible mechanisms of disease progression. Modern Pathology
602 **33:**2128-2138.

603 21. **Pannone G, Caponio VCA, De Stefano IS, Ramunno MA, Meccariello M,**
604 **Agostinone A, Pedicillo MC, Troiano G, Zhurakivska K, Cassano T, Bizzoca**
605 **ME, Papagerakis S, Buonaguro FM, Advani S, Muzio LL.** 2021. Lung
606 histopathological findings in COVID-19 disease – a systematic review. Infectious
607 Agents and Cancer **16:**34.

608 22. **Cameroni E, Bowen JE, Rosen LE, Saliba C, Zepeda SK, Culap K, Pinto D,**
609 **VanBlargan LA, De Marco A, di Iulio J, Zatta F, Kaiser H, Noack J, Farhat N,**

Czudnochowski N, Havenar-Daughton C, Sprouse KR, Dillen JR, Powell AE, Chen A, Maher C, Yin L, Sun D, Soriaga L, Bassi J, Silacci-Fregni C, Gustafsson C, Franko NM, Logue J, Iqbal NT, Mazzitelli I, Geffner J, Grifantini R, Chu H, Gori A, Riva A, Giannini O, Ceschi A, Ferrari P, Cippa PE, Franzetti-Pellanda A, Garzoni C, Halfmann PJ, Kawaoka Y, Hebner C, Purcell LA, Piccoli L, Pizzuto MS, Walls AC, Diamond MS, et al. 2022. Broadly neutralizing antibodies overcome SARS-CoV-2 Omicron antigenic shift. Nature **602:**664-670.

23. **Cao Y, Wang J, Jian F, Xiao T, Song W, Yisimayi A, Huang W, Li Q, Wang P, An R, Wang J, Wang Y, Niu X, Yang S, Liang H, Sun H, Li T, Yu Y, Cui Q, Liu S, Yang X, Du S, Zhang Z, Hao X, Shao F, Jin R, Wang X, Xiao J, Wang Y, Xie XS.** 2022. Omicron escapes the majority of existing SARS-CoV-2 neutralizing antibodies. Nature **602:**657-663.

24. **Wilhelm A, Widera M, Grikscheit K, Toptan T, Schenk B, Pallas C, Metzler M, Kohmer N, Hoehl S, Marschalek R, Herrmann E, Helfritz FA, Wolf T, Goetsch U, Ciesek S.** 2022. Limited neutralisation of the SARS-CoV-2 Omicron subvariants BA.1 and BA.2 by convalescent and vaccine serum and monoclonal antibodies. EBioMedicine **82:**104158.

25. **Pastorio C, Zech F, Noettger S, Jung C, Jacob T, Sanderson T, Sparrer KMJ, Kirchhoff F.** 2022. Determinants of Spike infectivity, processing, and neutralization in SARS-CoV-2 Omicron subvariants BA.1 and BA.2. Cell Host Microbe.

26. **Andeweg SP, de Gier B, Eggink D, van den Ende C, van Maarseveen N, Ali L, Vlaemynck B, Schepers R, Hahne SJM, Reusken C, de Melker HE, van den Hof S, Knol MJ.** 2022. Protection of COVID-19 vaccination and previous infection

against Omicron BA.1, BA.2 and Delta SARS-CoV-2 infections. Nat Commun **13:**4738.

27. **Shrestha LB, Foster C, Rawlinson W, Tedla N, Bull RA.** 2022. Evolution of the SARS-CoV-2 omicron variants BA.1 to BA.5: Implications for immune escape and transmission. Rev Med Virol**:**e2381.

28. **Hachmann NP, Miller J, Collier AY, Ventura JD, Yu J, Rowe M, Bondzie EA, Powers O, Surve N, Hall K, Barouch DH.** 2022. Neutralization Escape by SARS-CoV-2 Omicron Subvariants BA.2.12.1, BA.4, and BA.5. N Engl J Med **387:**86-88.

29. **Munoz-Fontela C, Dowling WE, Funnell SGP, Gsell PS, Riveros-Balta AX, Albrecht RA, Andersen H, Baric RS, Carroll MW, Cavaleri M, Qin C, Crozier I, Dallmeier K, de Waal L, de Wit E, Delang L, Dohm E, Duprex WP, Falzarano D, Finch CL, Frieman MB, Graham BS, Gralinski LE, Guilfoyle K, Haagmans BL, Hamilton GA, Hartman AL, Herfst S, Kaptein SJF, Klimstra WB, Knezevic I, Krause PR, Kuhn JH, Le Grand R, Lewis MG, Liu WC, Maisonnasse P, McElroy AK, Munster V, Oreshkova N, Rasmussen AL, Rocha-Pereira J, Rockx B, Rodriguez E, Rogers TF, Salguero FJ, Schotsaert M, Stittelaar KJ, Thibaut HJ, Tseng CT, et al.** 2020. Animal models for COVID-19. Nature **586:**509-515.

30. **Mykytyn AZ, Rissmann M, Kok A, Rosu ME, Schipper D, Breugem TI, van den Doel PB, Chandler F, Bestebroer T, de Wit M, van Royen ME, Molenkamp R, Oude Munnink BB, de Vries RD, GeurtsvanKessel C, Smith DJ, Koopmans MPG, Rockx B, Lamers MM, Fouchier R, Haagmans BL.** 2022. Antigenic cartography of SARS-CoV-2 reveals that Omicron BA.1 and BA.2 are antigenically distinct. Sci Immunol**:**eabq4450.

658 31. **Dhakal S, Ruiz-Bedoya CA, Zhou R, Creisher PS, Villano JS, Littlefield K,**
659 **Ruelas Castillo J, Marinho P, Jedlicka AE, Ordonez AA, Bahr M, Majewska N,**
660 **Betenbaugh MJ, Flavahan K, Mueller ARL, Looney MM, Quijada D, Mota F,**
661 **Beck SE, Brockhurst J, Braxton AM, Castell N, Stover M, D'Alessio FR,**
662 **Metcalf Pate KA, Karakousis PC, Mankowski JL, Pekosz A, Jain SK, Klein**
663 **SL, Johns Hopkins C-HSG.** 2021. Sex Differences in Lung Imaging and SARS-
664 CoV-2 Antibody Responses in a COVID-19 Golden Syrian Hamster Model. mBio
665 **12:**e0097421.
666 32. **Boyton RJ, Altmann DM.** 2021. The immunology of asymptomatic SARS-CoV-2
667 infection: what are the key questions? Nature Reviews Immunology **21:**762-768.
668 33. **Siggins MK, Thwaites RS, Openshaw PJM.** 2021. Durability of Immunity to
669 SARS-CoV-2 and Other Respiratory Viruses. Trends in Microbiology **29:**648-662.
670 34. **Sun F, Wang X, Tan S, Dan Y, Lu Y, Zhang J, Xu J, Tan Z, Xiang X, Zhou Y,**
671 **He W, Wan X, Zhang W, Chen Y, Tan W, Deng G.** 2021. SARS-CoV-2
672 Quasispecies Provides an Advantage Mutation Pool for the Epidemic Variants.
673 Microbiology Spectrum **9:**e00261-00221.
674 35. **Zhou P, Yang X-L, Wang X-G, Hu B, Zhang L, Zhang W, Si H-R, Zhu Y, Li B,**
675 **Huang C-L.** 2020. A pneumonia outbreak associated with a new coronavirus of
676 probable bat origin. nature **579:**270-273.
677 36. **Tran DP, Taira Y, Ogawa T, Misu R, Miyazawa Y, Kitao A.** 2022. Inhibition of
678 the hexamerization of SARS-CoV-2 endoribonuclease and modeling of RNA
679 structures bound to the hexamer. Sci Rep **12:**3860.
680 37. **Kindler E, Gil-Cruz C, Spanier J, Li Y, Wilhelm J, Rabouw HH, Zust R,**
681 **Hwang M, V'Kovski P, Stalder H, Marti S, Habjan M, Cervantes-Barragan L,**

Elliot R, Karl N, Gaughan C, van Kuppeveld FJ, Silverman RH, Keller M, Ludewig B, Bergmann CC, Ziebuhr J, Weiss SR, Kalinke U, Thiel V. 2017. Early endonuclease-mediated evasion of RNA sensing ensures efficient coronavirus replication. PLoS Pathog **13:**e1006195.

38. **Yuen CK, Lam JY, Wong WM, Mak LF, Wang X, Chu H, Cai JP, Jin DY, To KK, Chan JF, Yuen KY, Kok KH.** 2020. SARS-CoV-2 nsp13, nsp14, nsp15 and orf6 function as potent interferon antagonists. Emerg Microbes Infect **9:**1418-1428.

39. **Wu F, Zhao S, Yu B, Chen YM, Wang W, Song ZG, Hu Y, Tao ZW, Tian JH, Pei YY, Yuan ML, Zhang YL, Dai FH, Liu Y, Wang QM, Zheng JJ, Xu L, Holmes EC, Zhang YZ.** 2020. A new coronavirus associated with human respiratory disease in China. Nature **579:**265-269.

40. **Li X, Hou P, Ma W, Wang X, Wang H, Yu Z, Chang H, Wang T, Jin S, Wang X, Wang W, Zhao Y, Zhao Y, Xu C, Ma X, Gao Y, He H.** 2022. SARS-CoV-2 ORF10 suppresses the antiviral innate immune response by degrading MAVS through mitophagy. Cell Mol Immunol **19:**67-78.

41. **Yang DM, Lin FC, Tsai PH, Chien Y, Wang ML, Yang YP, Chang TJ.** 2021. Pandemic analysis of infection and death correlated with genomic open reading frame 10 mutation in severe acute respiratory syndrome coronavirus 2 victims. J Chin Med Assoc **84:**478-484.

42. **Liu Y, Soh WT, Kishikawa JI, Hirose M, Nakayama EE, Li S, Sasai M, Suzuki T, Tada A, Arakawa A, Matsuoka S, Akamatsu K, Matsuda M, Ono C, Torii S, Kishida K, Jin H, Nakai W, Arase N, Nakagawa A, Matsumoto M, Nakazaki Y, Shindo Y, Kohyama M, Tomii K, Ohmura K, Ohshima S, Okamoto T, Yamamoto M, Nakagami H, Matsuura Y, Nakagawa A, Kato T, Okada M,**

Standley DM, Shioda T, Arase H. 2021. An infectivity-enhancing site on the SARS-CoV-2 spike protein targeted by antibodies. Cell **184:**3452-3466 e3418.

43. **Wang TT, Sewatanon J, Memoli MJ, Wrammert J, Bournazos S, Bhaumik SK, Pinsky BA, Chokephaibulkit K, Onlamoon N, Pattanapanyasat K, Taubenberger JK, Ahmed R, Ravetch JV.** 2017. IgG antibodies to dengue enhanced for FcgammaRIIIA binding determine disease severity. Science **355:**395-398.

44. **Vennema H, de Groot RJ, Harbour DA, Dalderup M, Gruffydd-Jones T, Horzinek MC, Spaan WJ.** 1990. Early death after feline infectious peritonitis virus challenge due to recombinant vaccinia virus immunization. J Virol **64:**1407-1409.

45. **Weiss RC, Scott FW.** 1981. Antibody-mediated enhancement of disease in feline infectious peritonitis: comparisons with dengue hemorrhagic fever. Comp Immunol Microbiol Infect Dis **4:**175-189.

46. **Bourgonje AR, Abdulle AE, Timens W, Hillebrands JL, Navis GJ, Gordijn SJ, Bolling MC, Dijkstra G, Voors AA, Osterhaus AD, van der Voort PH, Mulder DJ, van Goor H.** 2020. Angiotensin-converting enzyme 2 (ACE2), SARS-CoV-2 and the pathophysiology of coronavirus disease 2019 (COVID-19). J Pathol **251:**228-248.

47. **Halstead SB, Katzelnick L.** 2020. COVID-19 Vaccines: Should We Fear ADE? J Infect Dis **222:**1946-1950.

48. **Altarawneh HN, Chemaitelly H, Hasan MR, Ayoub HH, Qassim S, AlMukdad S, Coyle P, Yassine HM, Al-Khatib HA, Benslimane FM, Al-Kanaani Z, Al-Kuwari E, Jeremijenko A, Kaleeckal AH, Latif AN, Shaik RM, Abdul-Rahim HF, Nasrallah GK, Al-Kuwari MG, Butt AA, Al-Romaihi HE, Al-Thani MH,**

Al-Khal A, Bertollini R, Tang P, Abu-Raddad LJ. 2022. Protection against the Omicron Variant from Previous SARS-CoV-2 Infection. N Engl J Med **386:**1288-1290.

49. **Rothberg MB, Kim P, Shrestha NK, Kojima L, Tereshchenko LG.** 2022. Protection Against the Omicron Variant Offered by Previous SARS-CoV-2 Infection: A Retrospective Cohort Study. Clin Infect Dis.

50. **Smid M, Berec L, Pribylova L, Majek O, Pavlik T, Jarkovsky J, Weiner J, Barusova T, Trnka J.** 2022. Protection by vaccines and previous infection against the Omicron variant of SARS-CoV-2. J Infect Dis.

51. **Oliviero A, de Castro F, Coperchini F, Chiovato L, Rotondi M.** 2021. COVID-19 Pulmonary and Olfactory Dysfunctions: Is the Chemokine CXCL10 the Common Denominator? Neuroscientist **27:**214-221.

52. **Iwata-Yoshikawa N, Shiwa N, Sekizuka T, Sano K, Ainai A, Hemmi T, Kataoka M, Kuroda M, Hasegawa H, Suzuki T, Nagata N.** 2022. A lethal mouse model for evaluating vaccine-associated enhanced respiratory disease during SARS-CoV-2 infection. Sci Adv **8:**eabh3827.

53. **Matsuyama S, Nao N, Shirato K, Kawase M, Saito S, Takayama I, Nagata N, Sekizuka T, Katoh H, Kato F, Sakata M, Tahara M, Kutsuna S, Ohmagari N, Kuroda M, Suzuki T, Kageyama T, Takeda M.** 2020. Enhanced isolation of SARS-CoV-2 by TMPRSS2-expressing cells. Proc Natl Acad Sci U S A **117:**7001-7003.

54. **Yamada S, Fukushi S, Kinoshita H, Ohnishi M, Suzuki T, Fujimoto T, Saijo M, Maeda K, Virus Diagnosis G.** 2021. Assessment of SARS-CoV-2 infectivity of upper respiratory specimens from COVID-19 patients by virus isolation using

754 VeroE6/TMPRSS2 cells. BMJ Open Respir Res **8**.

755 55. **Rodrigues MV, de Castro SO, de Albuquerque CZ, Mattaraia VGM, Santoro**
756 **ML.** 2017. The gingival vein as a minimally traumatic site for multiple blood
757 sampling in guinea pigs and hamsters. PLoS One **12:**e0177967.

758 56. **Zivcec M, Safronetz D, Haddock E, Feldmann H, Ebihara H.** 2011. Validation
759 of assays to monitor immune responses in the Syrian golden hamster (Mesocricetus
760 auratus). J Immunol Methods **368:**24-35.

761 57. **Quick J.** 2020. nCoV-2019 sequencing protocol v3 (LoCost), *on* Version created
762 by Josh Quick. https://protocols.io/view/ncov-2019-sequencing-protocol-v3-locost-
763 bh42j8ye. Accessed 11 Jul 2022.

764 58. **Itokawa K, Sekizuka T, Hashino M, Tanaka R, Kuroda M.** 2020. Disentangling
765 primer interactions improves SARS-CoV-2 genome sequencing by multiplex tiling
766 PCR. PLoS One **15:**e0239403.

767 59. **Itokawa K, Sekizuka T, Hashino M, Tanaka R, Eto S, Someno R, Kuroda M.**
768 2021. nCoV-2019 sequencing protocol for illumina. , *on* protocols.io.
769 https://protocols.io/view/ncov-2019-sequencing-protocol-for-illumina-b2msqc6e.
770 Accessed 11 Jul 2022.

771 60. **Itokawa K, Sasaki N.** 2021. Alt_nCov2019_primers_v0.11, *on* github.com.
772 https://github.com/ItokawaK/Alt_nCov2019_primers. Accessed 11 Jul 2022.

773

774

775

776 TABLE 1 SARS-CoV-2 variants in this study

Pango lineage (WHO label)	Sub lineage	Strain (Simplified name)	GISAID Accession no. of original isolate	Note
A		hCoV-19/Japan /TY-WK-521/2020 (WK-521)	EPI_ISL_408667	
B.1.1.7 (Alpha)		hCoV-19/Japan/QK002/2020 (QK002)	EPI_ISL_768526	
B.1.351 (Beta)		hCoV-19/Japan/TY8-612-P1/2021 (TY8-612)	EPI_ISL_1123289	
B.1.617.2 (Delta)		hCoV-19/Japan/TY11-927-P1/2021 (TY11-927)	EPI_ISL_2158617	
B.1.1.529 (Omicron)	BA.1.18	hCoV-19/Japan/TY38-873P0/2021 (TY38-873)	EPI_ISL_7418017	BA.1 + ORF1a:T1822I
B.1.1.529 (Omicron)	BA.1.1	hCoV-19/Japan/TY38-871P0/2021 (TY38-871)	EPI_ISL_7571618	
B.1.1.529 (Omicron)	BA.2	hCoV-19/Japan/TY40-385-P1/2022 (TY40-385)	EPI_ISL_9595859	
B.1.1.529 (Omicron)	BA.2.3	hCoV-19/Japan/TY40-816-P1/2022 (TY40-816)	EPI_ISL_9595861	BA.2 + S:A688V

777

778

779 FIGURE LEGENDS

780 **FIG 1 Experimental infection of hamsters with SARS-CoV-2 variants.** Study design
781 outlining experimental infections using 5-week-old female Syrian hamsters and SARS-
782 CoV-2 **(A)**. Body weight curve for 4 weeks after primary infection with SARS-CoV-2
783 variants. Dunnett's multiple comparison test compared with DMEM-inoculated animals (n
784 = 3 or 4). *, $P < 0.05$; **, $P < 0.01$ **(B)**. Neutralizing (NT) antibody titers against WK-521
785 (lineage A, black circle) or TY38-873 (lineage B.1.1.529, BA.1, **(C,** red circle)) strains in
786 the sera from hamsters at 4 weeks post-inoculation (p.i.). Data from the same animal are
787 connected with lines. *, $P < 0.05$ by Dunn's multiple comparison test following the
788 Kruskal–Wallis test **(C)**. Blocking activities of hamster sera between ACE2 and SARS-
789 CoV-2 spike was tested by the ACE2 binding inhibition ELISA using a V-Plex COVID-19
790 ACE2 neutralization kit (K15570U, Meso Scale Discovery) (n = 3 or 4). Each dot
791 represents data from an individual animal. Sera were diluted 1:10 (black dot) or 1:100
792 (black circle) for the analysis. Data from the same animal are connected with lines. *, $P <$
793 0.05; **, $P < 0.01$; ***, $P < 0.001$; ****, $P < 0.0001$ by Sidak's multiple comparison test
794 following two-way ANOVA **(D)**.
795
796 **FIG 2 Reinfection of hamsters with an Omicron variant.** Body weight curve during 3
797 days after second infection with an isolate of the TY38-873, B. 1.1.529 (Omicron)
798 subvariant BA.1 (n = 3 or 4) **(A)**. Bar graph showing the ratio of the chest organ weights
799 including lungs, trachea, heart, and thymus per body weight at 3 days p.i. (n = 3 or 4) **(B)**.
800 Bar graph showing virus titers **(C)** and virus-related RNA copies **(D)** in the nasal wash fluid
801 (upper panels) and supernatant from 10% lung tissue homogenates (lower panels) (n = 3 or
802 4). *, $P < 0.05$; **, $P < 0.01$; ***, $P < 0.001$; by Dunn's multiple comparison test following

803 the Kruskal–Wallis test. Percentage of animals with mutations involving amino acid
804 substitutions in each region **(E)**. The full-genome sequences of the Omicron BA.1 strains
805 recovered from the nasal wash fluid samples (n = 3 or 4). Brown bars in each panel indicate
806 the same data for the DMEM-BA.1 group.
807
808 **FIG 3 Histopathology and immunopathology of respiratory tract after reinfection**
809 **with an Omicron BA.1 variant.** Representative histopathological findings for the nasal
810 cavity epithelia and lungs of hamsters 3 days after second infection with an isolate of
811 TY38-873, B. 1.1.529 (Omicron) subvariant BA.1 (n = 4). H&E, hematoxylin and eosin
812 staining; IHC, immunohistochemistry for SARS-CoV-2 antigen detection. Br, bronchi.
813 Viral antigen-positive cells were mainly detected in the nasal epithelium on the cranial side.
814 Scale bars, 50 μm **(A)**. Distribution of viral antigens in nasal cavity and lungs by
815 immunohistochemistry. Heat map shows percentages of viral antigen-positive animals. SE;
816 squamous epithelium, RE; respiratory epithelium, OE; Olfactory epithelium, OB; Olfactory
817 bulb **(B)**. Viral antigen scores and pathological severity scores of lungs from hamsters (**C**
818 **and D**). Fibrin deposition scores of lungs by immunohistochemistry. Four lung lobes were
819 taken from each individual animal and scored to evaluate comprehensive pathological
820 changes. *$p < 0.05$ by one-way ANOVA **(E)**. Cytokine and chemokine levels in the nasal
821 wash fluid (upper panels) and supernatant from 10% lung tissue homogenates (lower
822 panels) of hamsters at 3 days p.i. (n = 3 or 4). *, $P < 0.05$ by Dunn's multiple comparison
823 test following the Kruskal–Wallis test **(F)**.
824
825 **FIG 4 Experimental infection of hamsters with Omicron subvariants.** Study design
826 outlining experimental infections using 5-week-old female Syrian hamsters and Omicron

827 subvariants **(A)**. Body weight curve for 4 weeks after primary inoculation with an isolate of
828 TY38-873, B. 1.1.529 (Omicron) subvariant BA.1. Control groups were inoculated with
829 cell culture medium (DMEM). No significant difference compared with DMEM-inoculated
830 animals (n = 16) was detected by Sidak's multiple comparison test following two-way
831 ANOVA **(B)**. Neutralizing (NT) antibody titers against TY38-873 (BA.1**,** left dots and
832 triangles) or TY40-385 (BA. 2, right dots and triangles) strains in the sera from hamsters on
833 4 weeks p.i. The dashed line indicates the limit of detection (<16). Each dot represents and
834 triangles data from an individual animal (n = 16). Data from the same samples are
835 connected with lines **(C)**. Blocking of interactions between ACE2 and SARS-CoV-2 spike
836 was tested by ACE2 binding inhibition ELISA using a V-Plex COVID-19 ACE2
837 neutralization kit (K15586U, Meso Scale Discovery) (n = 16). Sera were diluted 1:10 or
838 1:100 for the analysis. **, $P < 0.01$; ****, $P < 0.0001$ by Sidak's multiple comparison test
839 following two-way ANOVA **(D)**. Body weight curve during 3 days after primary or
840 reinfection with subvariants of B. 1.1.529. (n = 4). No significant differences were detected
841 between the primary (black lines) and reinfection (red lines) groups by two-way ANOVA
842 **(E)**. Bar graph showing the ratios of the weights of the chest organ including lungs, trachea,
843 heart, and thymus to body weights at 3 days p.i *, $P < 0.05$ by Mann-Whitney test **(F)**. Bar
844 graph of virus titers in the nasal wash fluid (upper panels) and supernatant from 10% lung
845 tissue homogenates (lower panels) **(G)**. Dot line indicates detection limit. *, $P < 0.05$ by
846 Mann-Whitney test., Black lines/bars indicate the primary infection groups and red
847 lines/bars are from the reinfection groups (E-G).
848
849 **FIG 5 Impact of reinfection in hamsters with Omicron subvariants.** Bar graph showing
850 virus-related RNA copies in the nasal wash fluid (upper panels) and supernatant from 10%

851 lung tissue homogenates (lower panels). Dot line indicates detection limit. *, $P < 0.05$ by
852 Mann-Whitney test. B-D, black bars indicate the primary infection groups and red bars the
853 reinfection groups **(A)**. Percentage of animals with mutations involving amino acid
854 substitutions in each region. Comparison of mutations detected in animals reinfected with
855 SARS-CoV-2. The full-genome sequences of the B. 1.1.529 subvariants recovered from the
856 nasal wash fluid samples (n = 4 per group) were determined using NGS analyses **(B)**.
857
858 **FIG 6 Histopathology of respiratory tract tissues from hamsters following primary- or**
859 **reinfection with Omicron subvariants.** Representative histopathological findings of the
860 nasal cavity and lungs from hamsters after primary or second infection with subvariants of
861 B. 1.1.529 (Omicron) (n = 4) **(A)**. H&E, hematoxylin and eosin staining; IHC,
862 immunohistochemistry for SARS-CoV-2 antigen detection. Br, bronchi. Viral antigen-
863 positive cells were mainly detected in the nasal epithelium on the cranial side. Scale bars,
864 50 μm. Distribution of viral antigen in respiratory tract from hamsters **(B)**. Heat map shows
865 percentage of viral antigen-positive animals. SE; squamous epithelium, RE; respiratory
866 epithelium, OE; Olfactory epithelium, OB; Olfactory bulb. Viral antigen scores and
867 pathological severity scores of lungs in hamsters **(C and D)**. Fibrin deposition scores of
868 lungs from hamsters by immunohistochemistry. Four lung lobes were taken from each
869 individual animal and scored. *$p < 0.05$ by one-way ANOVA **(E)**.
870
871 **Supplementary Figure 1. Histopathology of respiratory tract tissues after reinfection**
872 **with an Omicron BA.1 variant.** Representative histopathological findings of the nasal
873 cavity and lungs from hamsters 3 days after second infection with an isolate of TY38-873,
874 B. 1.1.529 (Omicron) subvariant BA.1 (n = 3 or 4). H&E, hematoxylin and eosin staining;

875 IHC, immunohistochemistry for SARS-CoV-2 antigen detection. Br, bronchi. Viral antigen-
876 positive cells were mainly detected in the nasal epithelium on the cranial side. Scale bars,
877 50 μm.
878
879 **Supplementary Figure 2. Cytokine and chemokine levels in the respiratory airway of**
880 **hamsters 3 days post primary or reinfection.** The nasal wash fluid **(A)** and supernatant
881 from 10% lung tissue homogenates **(B)** of hamsters at 3 days p.i. (n = 4) *, $P < 0.05$ by
882 Mann-Whitney test. Black bars indicate the first infection group; red bars, reinfection
883 group. Dashed line indicates mean values in the nasal wash fluid or lung homogenates from
884 mock-infected hamsters (n = 4, at 3 days p.i. with DMEM).

Figure 1

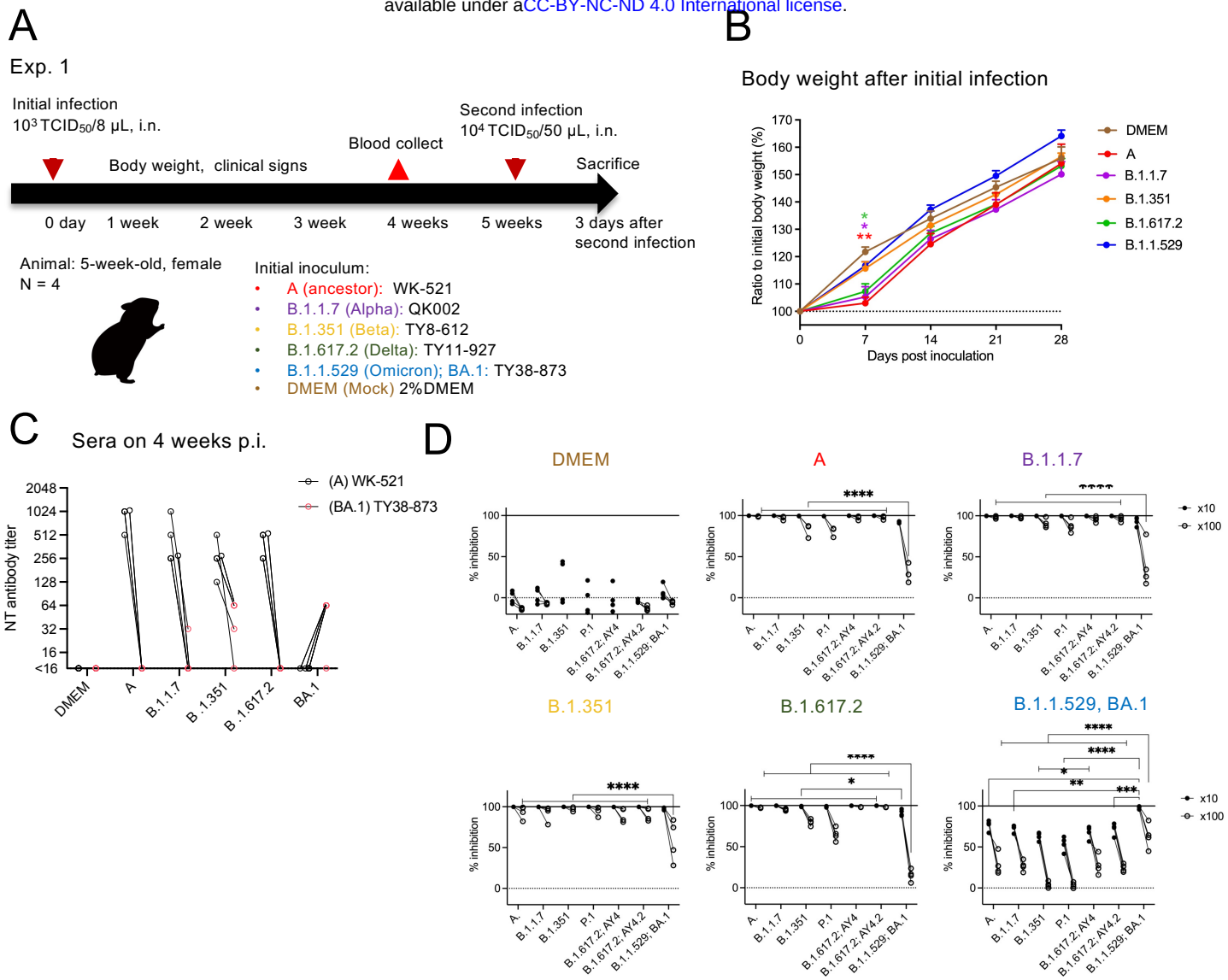

Figure 2

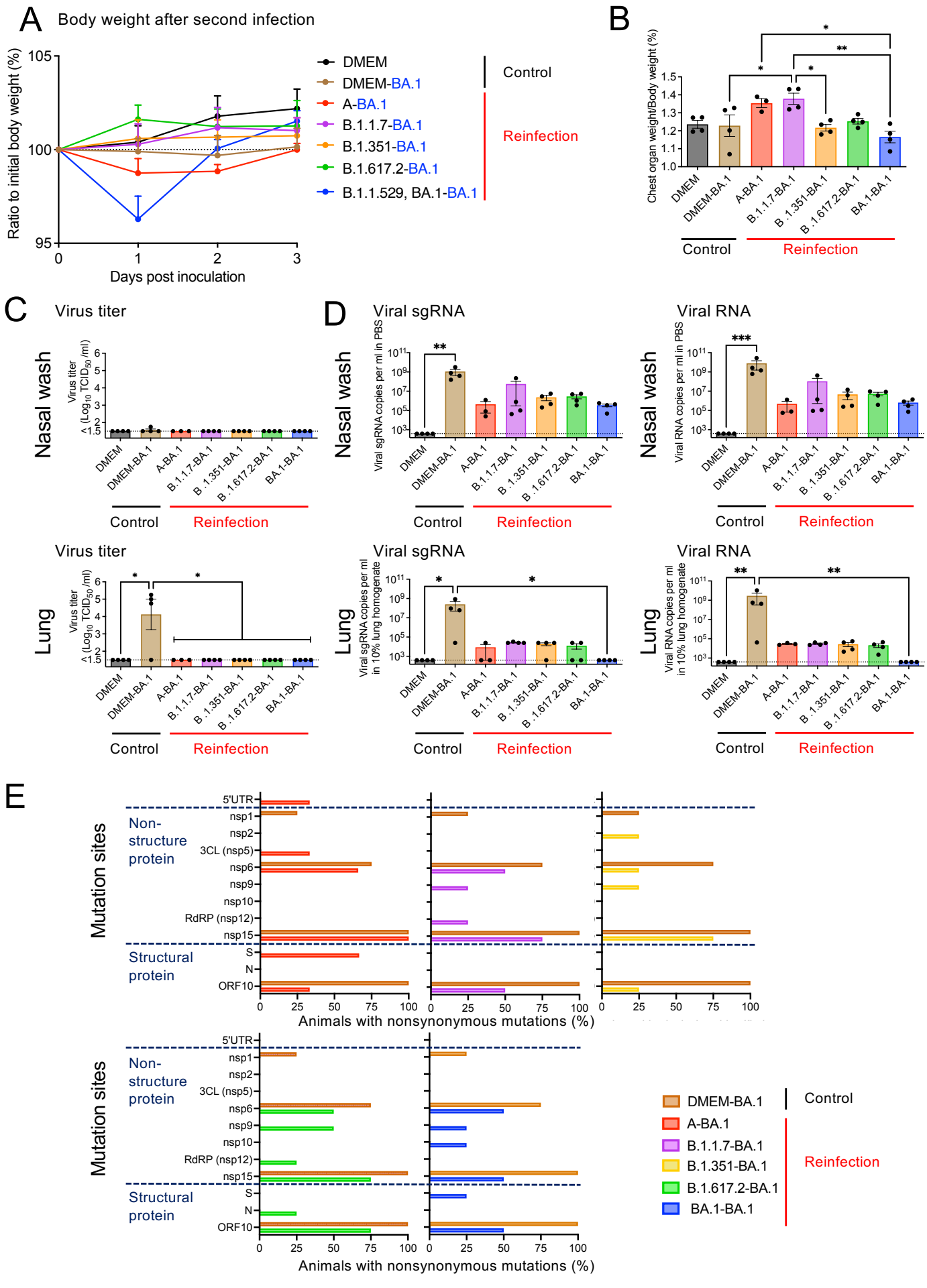
A
Body weight after second infection
Ratio to initial body weight (%)
Days post inoculation
DMEM
DMEM-BA.1
A-BA.1
B.1.1.7-BA.1
B.1.351-BA.1
B.1.617.2-BA.1
B.1.1.529, BA.1-BA.1
Control
Reinfection
B
Chest organ weight/Body weight (%)
C
Virus titer
Nasal wash
Lung
D
Viral sgRNA
Viral RNA
Viral sgRNA copies per ml in PBS
Viral RNA copies per ml in PBS
Viral sgRNA copies per ml in 10% lung homogenate
Viral RNA copies per ml in 10% lung homogenate
E
Mutation sites
Non-structure protein
Structural protein
5'UTR
nsp1
nsp2
3CL (nsp5)
nsp6
nsp9
nsp10
RdRP (nsp12)
nsp15
S
N
ORF10
Animals with nonsynonymous mutations (%)

Figure 3

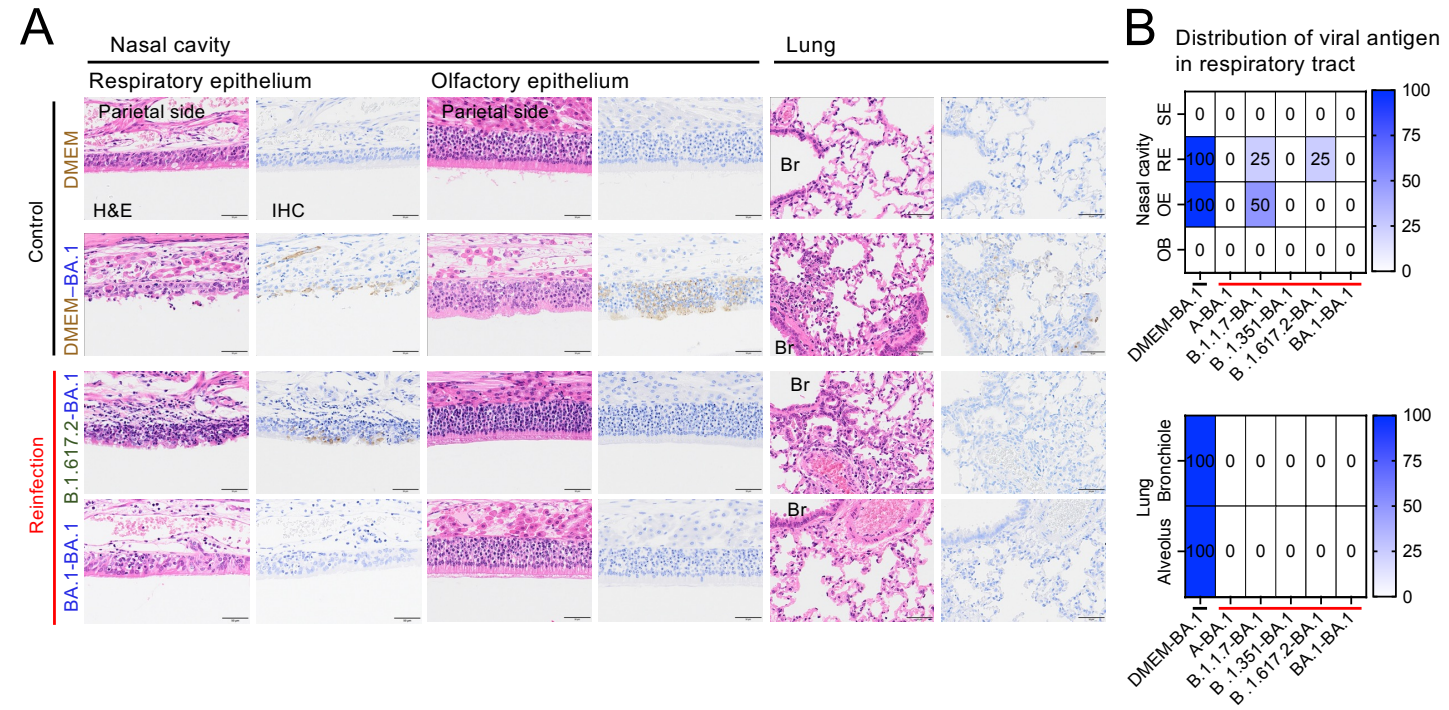
A
Nasal cavity
Lung
Respiratory epithelium
Olfactory epithelium
Parietal side
Parietal side
Control
DMEM
DMEM–BA.1
Reinfection
B.1.617.2-BA.1
BA.1-BA.1
H&E
IHC
Br
B
Distribution of viral antigen in respiratory tract
Nasal cavity
SE
RE
OE
OB
Lung
Bronchiole
Alveolus
DMEM-BA.1
A-BA.1
B.1.1.7-BA.1
B.1.351-BA.1
B.1.617.2-BA.1
BA.1-BA.1

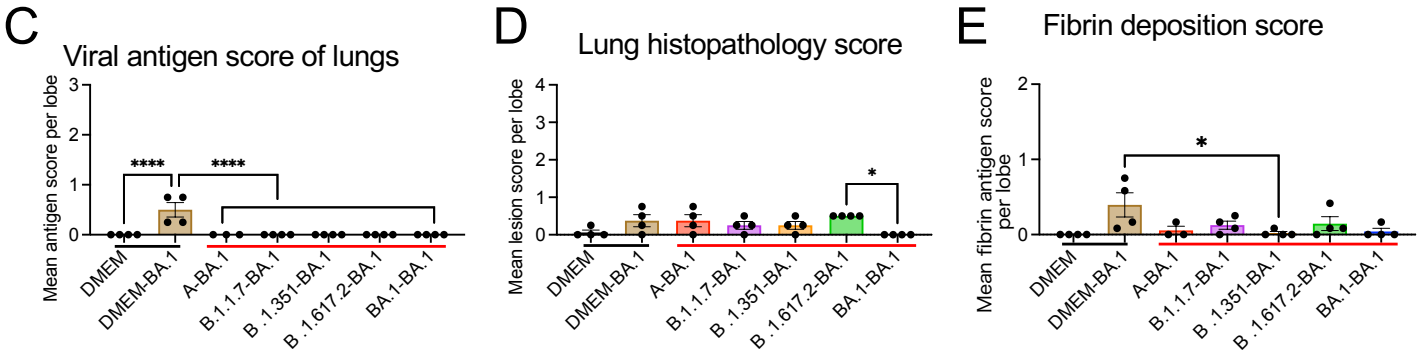
C
Viral antigen score of lungs
Mean antigen score per lobe
D
Lung histopathology score
Mean lesion score per lobe
E
Fibrin deposition score
Mean fibrin antigen score per lobe
DMEM
DMEM-BA.1
A-BA.1
B.1.1.7-BA.1
B.1.351-BA.1
B.1.617.2-BA.1
BA.1-BA.1

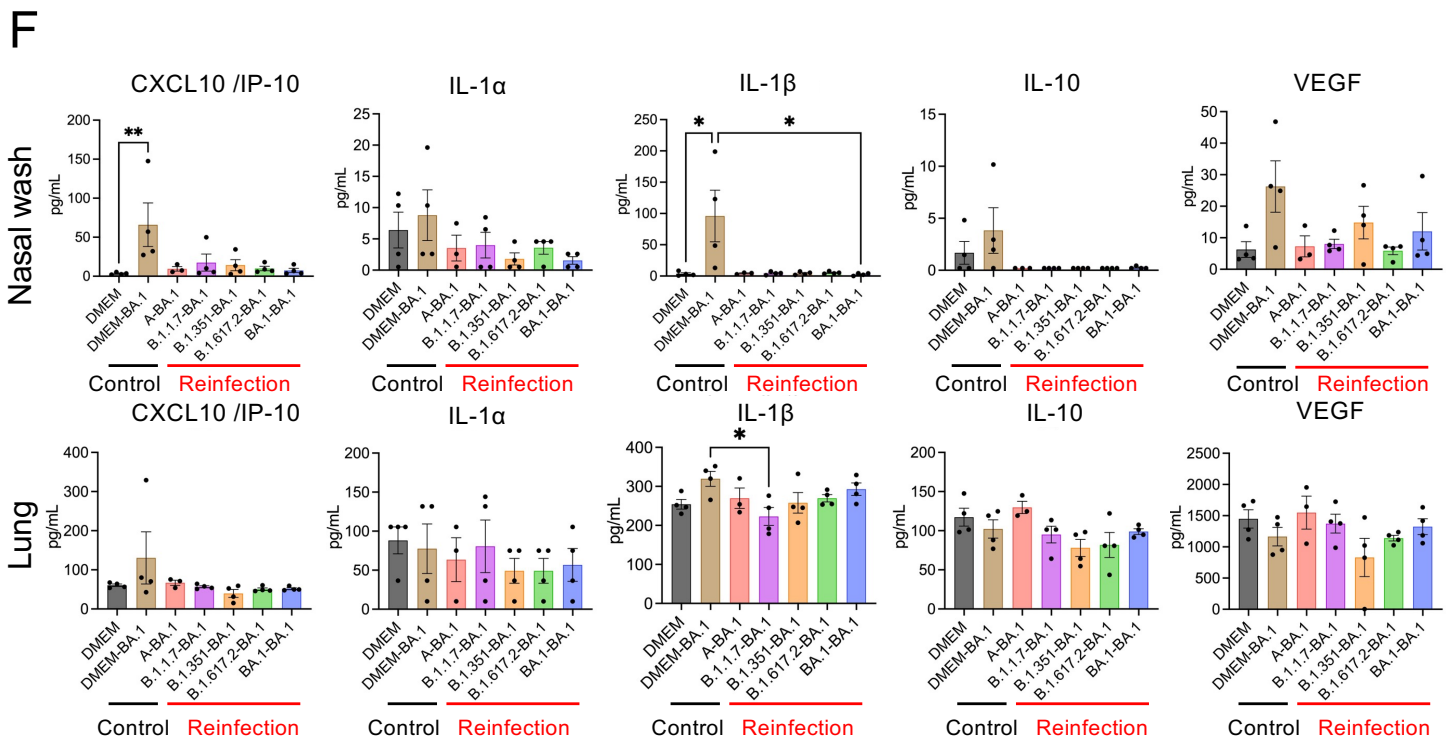
F
Nasal wash
Lung
CXCL10 /IP-10
IL-1α
IL-1β
IL-10
VEGF
pg/mL
Control
Reinfection

Figure 4

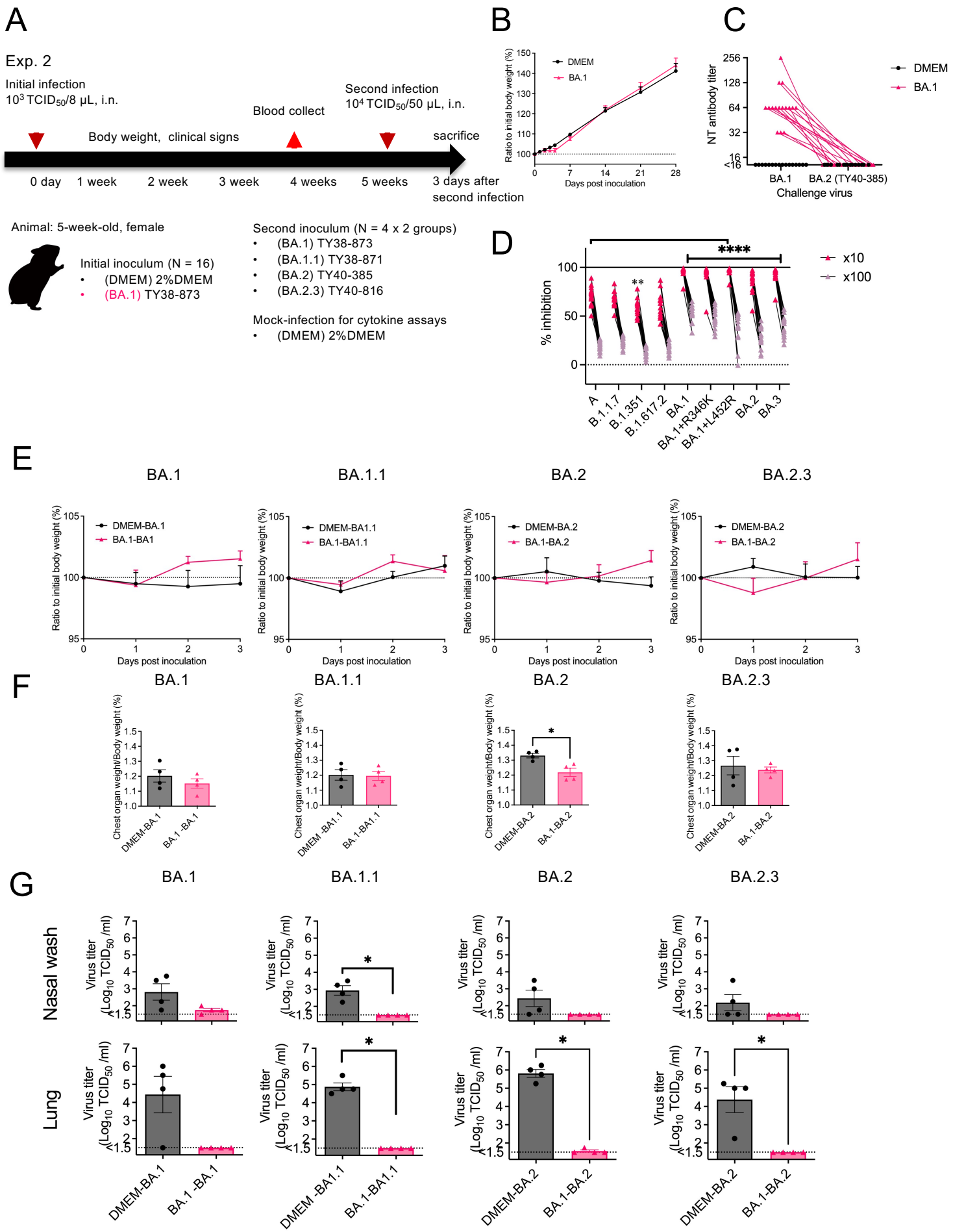
A
Exp. 2
Initial infection
10³ TCID50/8 μL, i.n.
Blood collect
Second infection
10⁴ TCID50/50 μL, i.n.
Body weight, clinical signs
sacrifice
0 day
1 week
2 week
3 week
4 weeks
5 weeks
3 days after second infection
Animal: 5-week-old, female
Initial inoculum (N = 16)
(DMEM) 2%DMEM
(BA.1) TY38-873
Second inoculum (N = 4 x 2 groups)
(BA.1) TY38-873
(BA.1.1) TY38-871
(BA.2) TY40-385
(BA.2.3) TY40-816
Mock-infection for cytokine assays
(DMEM) 2%DMEM
B
Ratio to initial body weight (%)
DMEM
BA.1
Days post inoculation
C
NT antibody titer
DMEM
BA.1
BA.1
BA.2 (TY40-385)
Challenge virus
D
% inhibition
x10
x100
A
B.1.1.7
B.1.351
B.1.617.2
BA.1
BA.1+R346K
BA.1+L452R
BA.2
BA.3
E
BA.1
BA.1.1
BA.2
BA.2.3
Ratio to initial body weight (%)
DMEM-BA.1
BA.1-BA1
DMEM-BA1.1
BA.1-BA1.1
DMEM-BA.2
BA.1-BA.2
Days post inoculation
F
BA.1
BA.1.1
BA.2
BA.2.3
Chest organ weight/Body weight (%)
DMEM-BA.1
BA.1 -BA.1
DMEM-BA1.1
BA.1-BA1.1
DMEM-BA.2
BA.1-BA.2
G
BA.1
BA.1.1
BA.2
BA.2.3
Nasal wash
Lung
Virus titer (Log10 TCID50 /ml)
DMEM-BA.1
BA.1 -BA.1
DMEM -BA1.1
BA.1-BA1.1
DMEM-BA.2
BA.1-BA.2

Figure 5

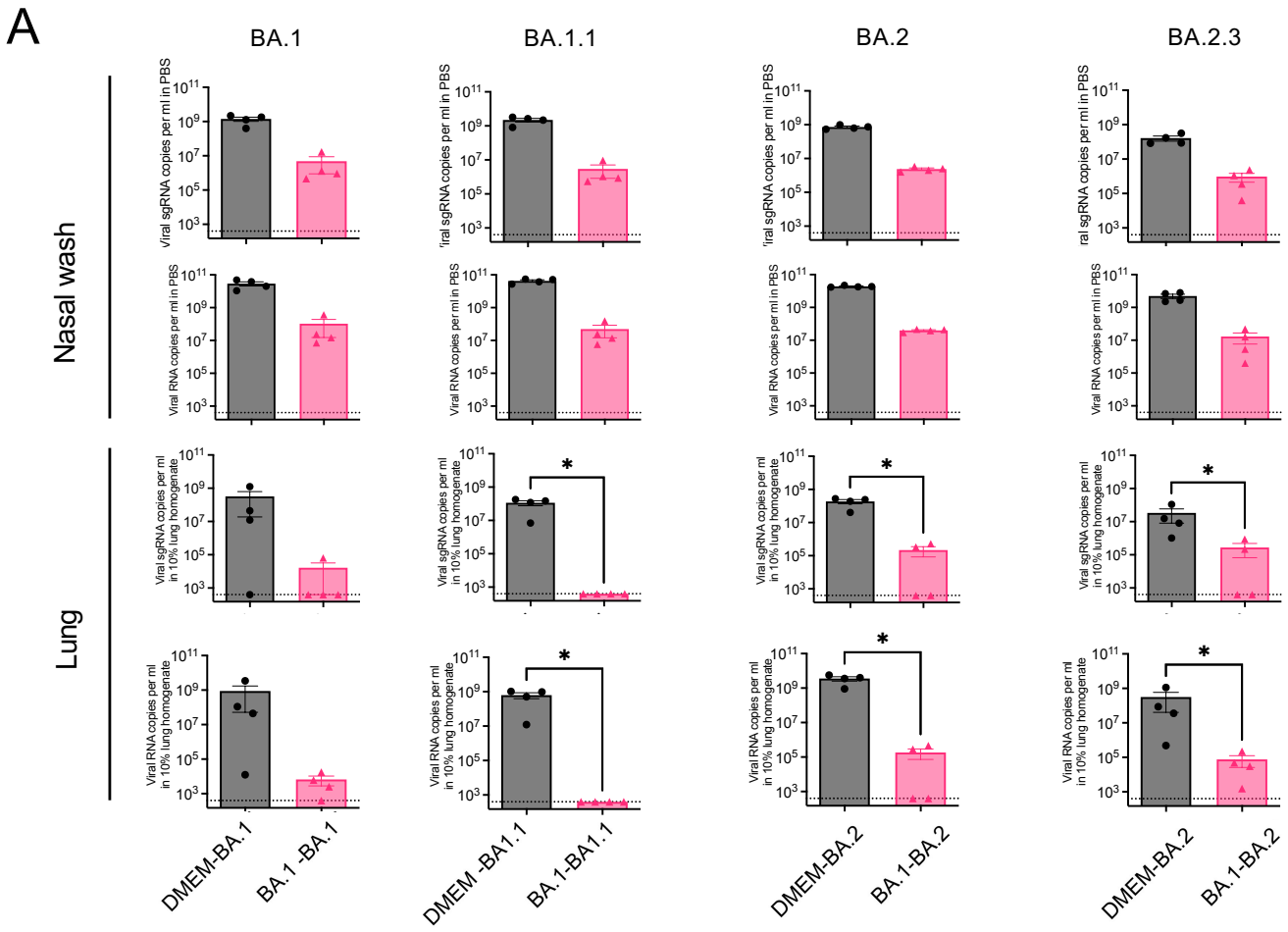
A
BA.1
BA.1.1
BA.2
BA.2.3
Nasal wash
Lung
Viral sgRNA copies per ml in PBS
Viral RNA copies per ml in PBS
Viral sgRNA copies per ml in 10% lung homogenate
Viral RNA copies per ml in 10% lung homogenate
*
DMEM-BA.1
BA.1 -BA.1
DMEM -BA1.1
BA.1-BA1.1
DMEM-BA.2
BA.1-BA.2
DMEM-BA.2
BA.1-BA.2

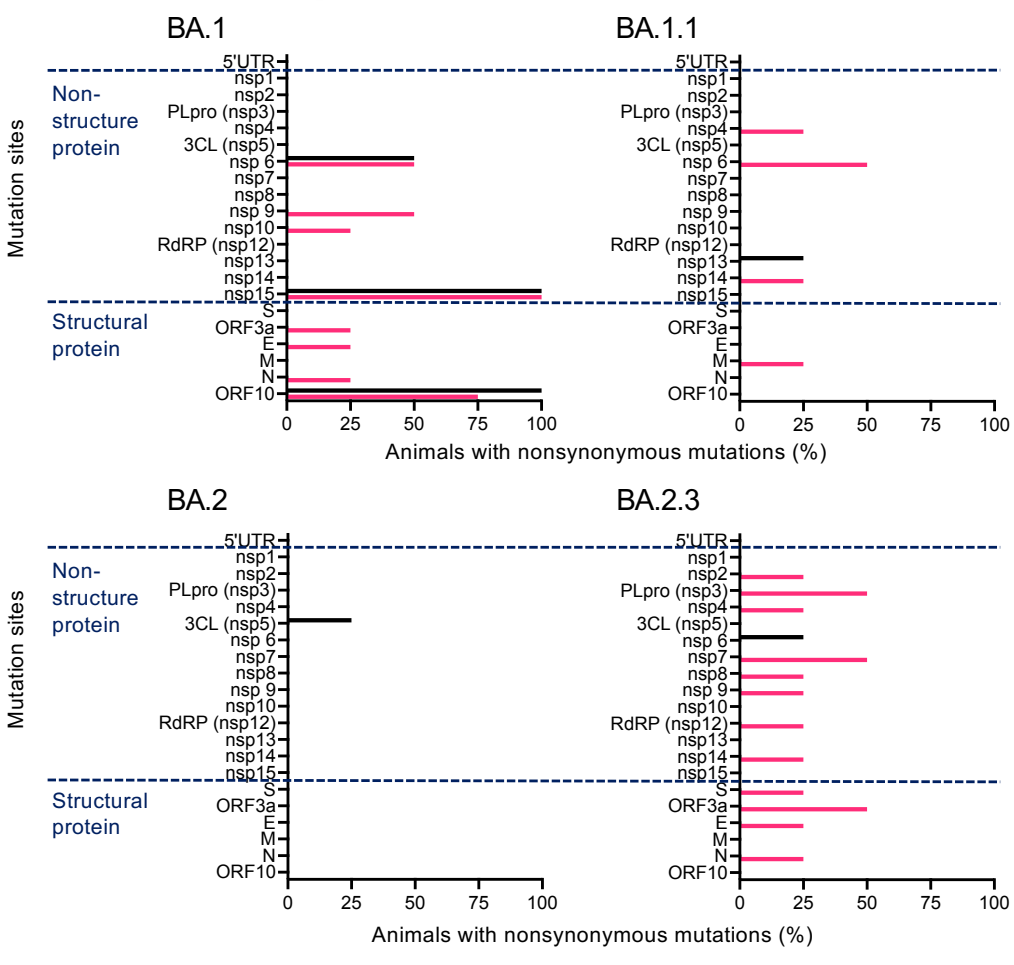
B
BA.1
BA.1.1
BA.2
BA.2.3
Mutation sites
Non-structure protein
Structural protein
5'UTR
nsp1
nsp2
PLpro (nsp3)
nsp4
3CL (nsp5)
nsp 6
nsp7
nsp8
nsp 9
nsp10
RdRP (nsp12)
nsp13
nsp14
nsp15
S
ORF3a
E
M
N
ORF10
0
25
50
75
100
Animals with nonsynonymous mutations (%)

Figure 6

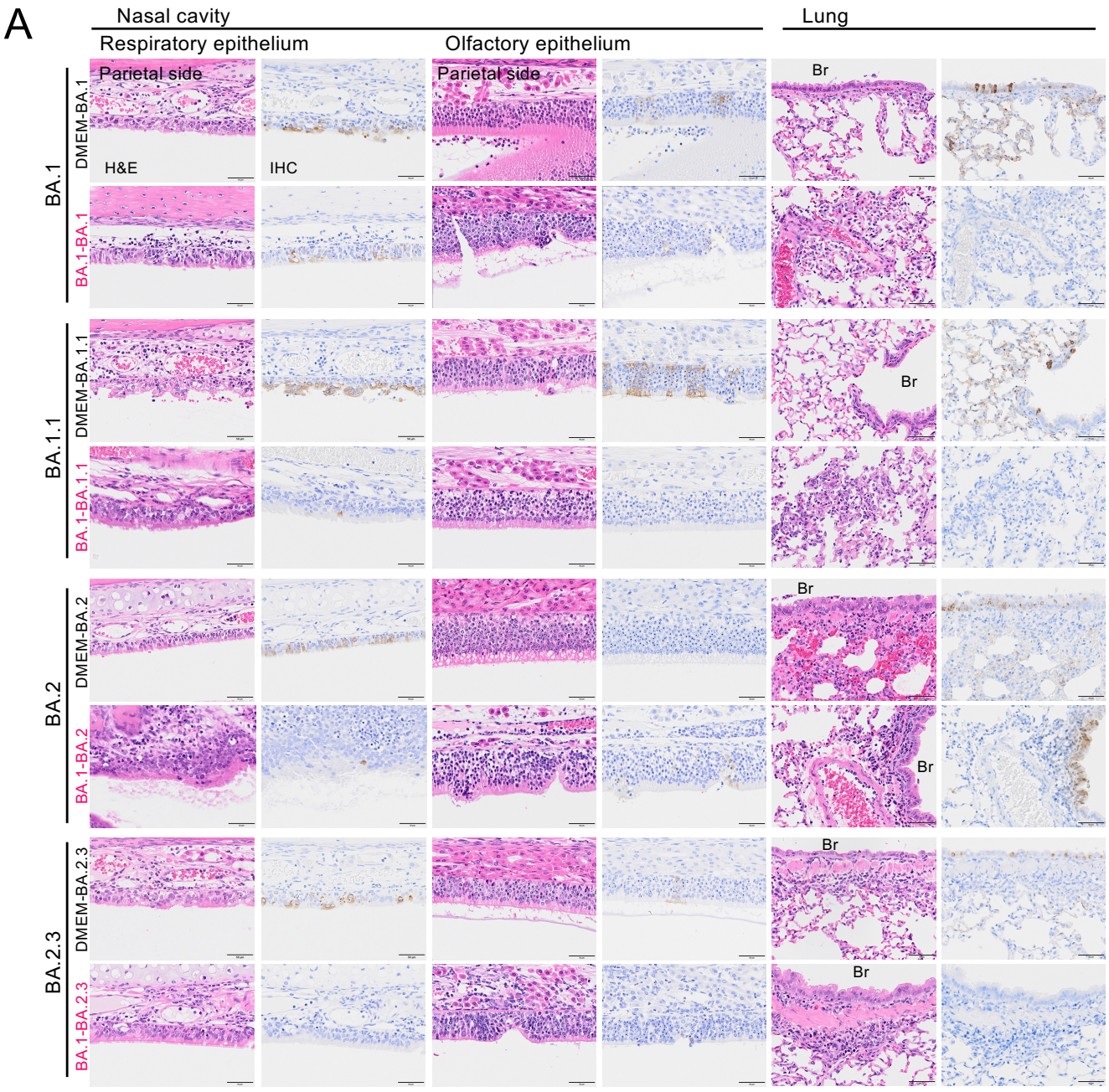
A
Nasal cavity
Lung
Respiratory epithelium
Olfactory epithelium
Parietal side
Parietal side
Br
H&E
IHC
BA.1
DMEM-BA.1
BA.1-BA.1
BA.1.1
DMEM-BA.1.1
BA.1-BA.1.1
BA.2
DMEM-BA.2
BA.1-BA.2
BA.2.3
DMEM-BA.2.3
BA.1-BA.2.3

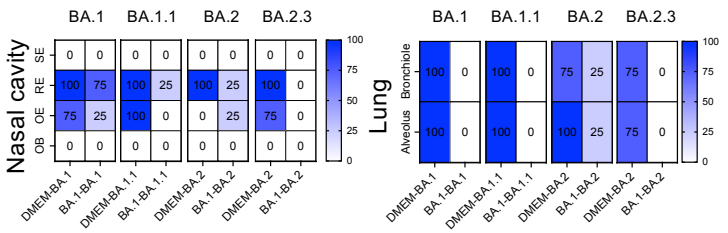
B
Distribution of viral antigen in respiratory tract
BA.1
BA.1.1
BA.2
BA.2.3
Nasal cavity
SE
RE
OE
OB
Lung
Bronchiole
Alveolus
DMEM-BA.1
BA.1-BA.1
DMEM-BA.1.1
BA.1-BA.1.1
DMEM-BA.2
BA.1-BA.2
DMEM-BA.2
BA.1-BA.2

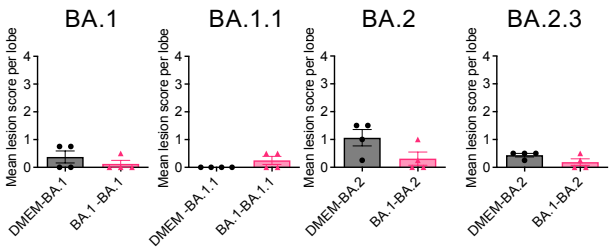
D
Lung histopathology score
BA.1
BA.1.1
BA.2
BA.2.3
Mean lesion score per lobe
DMEM-BA.1
BA.1-BA.1
DMEM-BA.1.1
BA.1-BA.1.1
DMEM-BA.2
BA.1-BA.2
DMEM-BA.2
BA.1-BA.2

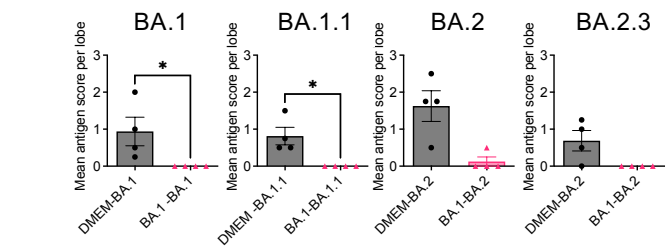
C
Viral antigen score of lungs
BA.1
BA.1.1
BA.2
BA.2.3
Mean antigen score per lobe
*
*
DMEM-BA.1
BA.1 -BA.1
DMEM -BA.1.1
BA.1-BA.1.1
DMEM-BA.2
BA.1-BA.2
DMEM-BA.2
BA.1-BA.2

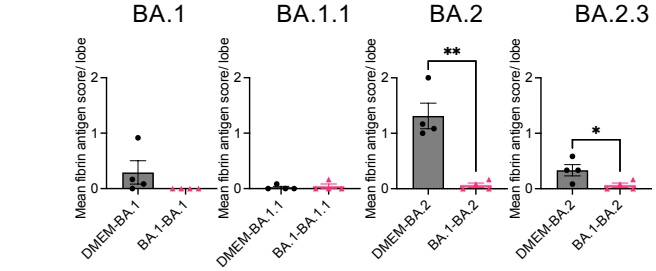
E
Fibrin deposition score
BA.1
BA.1.1
BA.2
BA.2.3
Mean fibrin antigen score/ lobe
**
*
DMEM-BA.1
BA.1-BA.1
DMEM-BA.1.1
BA.1-BA.1.1
DMEM-BA.2
BA.1-BA.2
DMEM-BA.2
BA.1-BA.2

Supplementary Figure 1

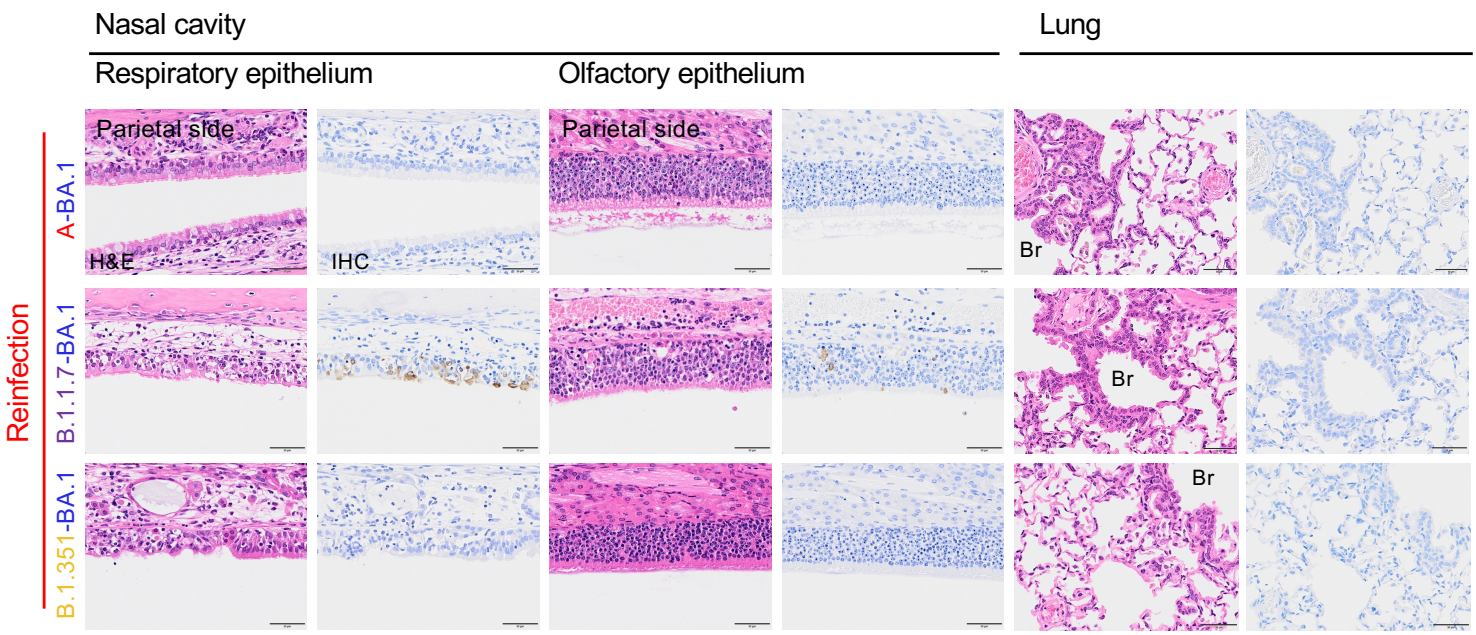

Supplementary Figure 2

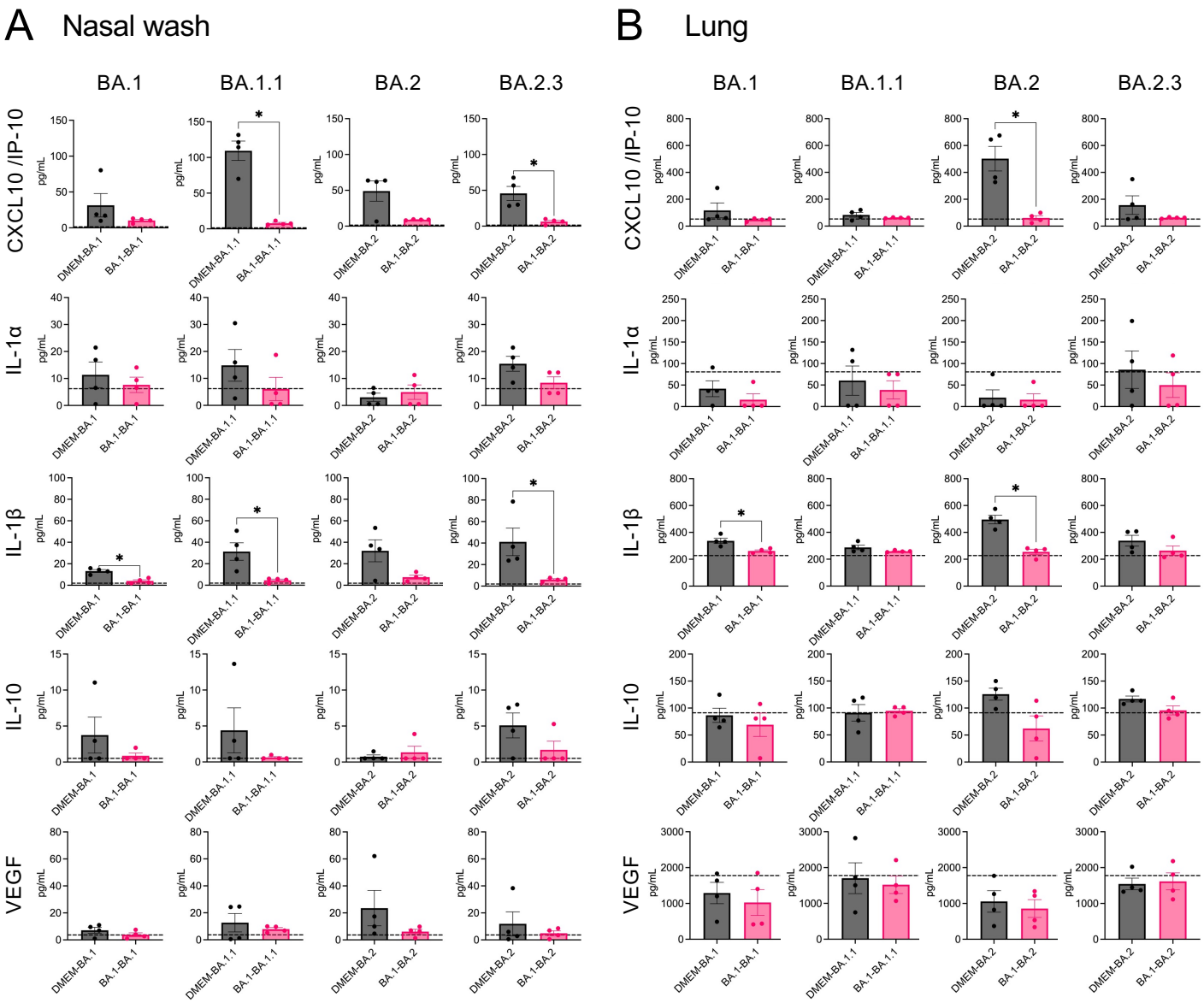

Table S1

Variant			DMEM-BA1				A-BA.1				B.1.1.7-BA.1				B.1.351-BA.1				B.1.617.2-BA.1				B.1.1.529, BA.1-BA.1			
Nuc no. in Wuhan	AA substitution	protein	1	2	3	4	5	6	7	8	9	10	11	12	13	14	15	16	17	18	19	20	21	22	23	24
209T	Silent	-						Y																		
								C:44.2%																		
804G	ORF1a: G180E	nsp1:G180E		R																						
				A:12.8%																						
921T	ORF1a: L219Q	nsp2:L39Q													W											
															A:33.1%											
1915C	Silent	nsp2									Y															
											T:13.0%															
7051C	Silent	PLpro (nsp3)							Y																	
									T:24.9%																	
7945C	Silent	PLpro (nsp3)												Y												
														T:33.3%												
9451C	Silent	nsp4													Y											
															T:17.3%											
9970A	Silent	nsp4									R															
											G:45.1%															
10934T	ORF1a: F3557L	3CL (nsp5): F294L						Y																		
								C:37.6																		
11020C	Silent	nsp6							Y																	
									T:28.7%																	
11083G	ORF1a: L3606F	nsp6:L37F																					K			
																							T:11.4%			
11355C	ORF1a: A3697V	nsp6:A128V														Y										
																T:33.0%										
11674C	Silent	nsp6										Y														
												T:21.5%														
11750C	ORF1a: L3829F	nsp6:L260F	Y	Y	Y		Y		Y			Y							Y			Y	Y		Y	
			T:15.5%	T:36.4%	T:12.5%		T:13.7%		T:39.4%			T:51.3%							T:45.4%			T:10.5%	T:12.0%		T:19.3%	
12747C	ORF1a: T4161I	nsp9:T21I									Y						Y									
											T:13.6%						T:23.6%									
12884A	ORF1a: T4207A	nsp9:T67A																		R		R		R		
																				G:20.6%		G:10.5%		G:73.1%		
13131A	ORF1a: Q4289R	nsp10:Q36R																							R	
																									G:35.2%	
15211A	ORF1b: T582A	RdRP (nsp12): T591A												R								R				
														G:10.5%								G:36.6%				
19206C	Silent	nsp14																							Y	
																									T:28.9%	
20486A	ORF1b: K2340T	nsp15:K289T	M	M	M	M	M	M	M			M	C	M		M	M	M	M		C	M	M		M	
			C:39.6%	C:35.8%	C:46.3%	C:40.9%	C:38.4%	C:12.0%	C:77.2%			C:30.1%	C:95.6%	C:26.5%		C:46.8%	C:24.2%	C:69.1%	C:24.5%		100%	C:16.4%	C:50.8%		C:24.0%	
21561C	Silent	-																						Y		
																								T:10.2%		
21562A	Silent	-																						W		
																								T:10.2%		
21565G	S: M1 del	S: M1 del																						R		
																								A:10.1%		
21925T	Silent	S													Y											
															C:56.7%											
22151A	S: I197L	S: I197L						M																		
								C:40.9%																		
22194A	S: N211del, L212I	S:N211I, L212del					A/del																			
							A:15.1%																			
22195T							T/del																			
							T:15.1%																			
22196T							T/del																			
							T:15.1%																			
23788T	Silent	S																							Y	
																									C:34.9%	
28971A	N: K233R	N: K233R																				R				
																						G:12.1%				
29645G	ORF10: V30L	ORF10: V30L	K	K	K	K	K				K	K					K		K	K		K		K	K	
			G:28.4%	G:23.1%	G:22.1%	G:22.4%	T:74.2%				T:16.8%	T:78.1%					G:50.3%		G:13.3%	G:21.5%		G:21.6%		G:10.7%	G:50.3%	

Table S2

Variant			Inoculum		Group/Animal No.				Inoculum		Group/Animal No.			
			1st	2nd	DMEM-BA.1				1st	2nd	BA.1-BA.1			
Nuc no. in Wuhan	AA substitution	protein	DMEM	TY38-873	1	2	3	4	TY38-873	TY38-873	17	18	19	20
11048G	ORF1a: V3595F	nsp6:V26F		G					G	G				K
														T:11.1%
11750C	ORF1a: L3829F	nsp6:L260F		C	Y			Y	C	C		Y		
					T:12.9%			T:15.9%				T:37.7%		
12747C	ORF1a: T4161I	nsp9:T21I		C					C	C	Y	Y		
											T:17.8%	T:13.0%		
13131A	ORF1a: Q4289R	nsp10:Q36R		A					A	A	R			
											G:29.0%			
20486A	ORF1b: K2340T	nsp15:K289T		A	M	M	M	M	A	A	M	M	M	M
					C:46.5%	C:45.0%	C:49.9%	C:46.1%			C:34.5%	C:24.3%	C:89.8%	C:44.7%
25487C	ORF3a: T32I	ORF3a:T32I		C					C	C		Y		
												T:11.8%		
26263G	E: E7K	E: E7K		G					G	G		R		
												A:10.4%		
28391C	N: R40C	N: R40C		C					C	C	Y			
											T:23.1%			
29645G	ORF10: V30L	ORF10: V30L		T	K	K	K	K	T	T	K	K		K
					G:19.3%	G:22.5%	G:16.2%	G:19.6%			G:32.6%	G:52.8%		G:30.0%
PANGO				BA.1.18	BA.1.18	BA.1.18	BA.1.18	BA.1.18	BA.1.18	BA.1.18	BA.1.18	BA.1.18	BA.1.18	BA.1.18

Variant			Inoculum		Group/Animal No.				Inoculum		Group/Animal No.			
			1st	2nd	DMEM-BA.1.1				1st	2nd	BA.1-BA.1.1			
Nuc no. in Wuhan	AA substitution	protein	DMEM	TY38-871	5	6	7	8	TY38-873	TY38-871	21	22	23	24
9005G	ORF1a: V2914I	nsp4:V151I		G					G	G	R			
											A:13.6%			
11355C	ORF1a: A3697V	nsp6:A128V		C					C	C				Y
														T:35.8%
11516G	ORF1a: V3751I	nsp6:V182I		G					G	G	R			
											A:31.4%			
17977C	ORF1b: L1504F	nsp13:L581F		C		Y			C	C				
						T:21.6%								
19284T	ORF1b: D1939E	nsp14:D415E		T					T	T				W
														A:34.8%
26536A	M: N5S	M:N5S		A					A	A			R	
													G:31.5%	
PANGO			-	BA.1.1	BA.1.1	BA.1.1	BA.1.1	BA.1.1	BA.1.18	BA.1.1	BA.1.1	BA.1.1	BA.1.1	BA.1.1

Variant			Inoculum		Group/Animal No.				Inoculum		Group/Animal No.			
			1st	2nd	DMEM-BA.2				1st	2nd	BA.1-BA.2			
Nuc no. in Wuhan	AA substitution	protein	DMEM	TY40-385	9	10	11	12	TY38-873	TY40-385	25	26	27	28
10512A	ORF1a: D3416G	3CLpro:D153G	-	A				R	A	A				
								G:10.3%						
28471C	Silent	N		C					C	C				Y
														T:10.7%
PANGO				BA.2	BA.2	BA.2	BA.2	BA.2	BA.1.18	BA.2	BA.2	BA.2	BA.2	BA.2

Variant			Inoculum		Group/Animal No.				Inoculum		Group/Animal No.			
			1st	2nd	DMEM-BA.2.3				1st	2nd	BA.1-BA.2.3			
Nuc no. in Wuhan	AA substitution	protein	DMEM	TY40-816	13	14	15	16	TY38-873	TY40-816	29	30*	31	32
3784C	Silent	nsp3		C					C	C	Y			
											T:18.3%			
7093C	Silent	nsp3		C					C	C				Y
														T:13.0%
7317T	ORF1a: F2351S	nsp3: F1533S		T					T	T	Y			
											C:44.6%			
11750C	ORF1a: L3829F	nsp6:L260F		C			Y		C	C				
							T:21.4%							
12060A	ORF1a: E3932A	nsp7:G73A		A					A	A				M
														C:37.3%
26198C	ORF3a: T269M	ORF3a:T269M		C					C	C				Y
														T:14.2%
PANGO				BA.2.3	BA.2.3	BA.2.3	BA.2.3	BA.2.3	BA.1.18	BA.2.3	BA.2.3	BA.2.3	BA.2.3	BA.2.3

*Animal No.30 had other mutations. See Supplementary Table3

Table S3

			Inoculum		Group/Animal No.
14-3, ham#29-32 1st: TY38-873, 2nd: TY40-816			1st	2nd	BA.1-BA.2.3
Nuc no. in Wuhan	AA substitution	Protein	TY38-873	TY40-816	30
2086G	ORF1a: Q607H	nsp2: Q427H	G	G	K T:10.9%
4250T	ORF1a: Y1329H	nsp3: Y511H	T	T	Y C:15.2%
5514T	ORF1a: V1750A	nsp3: V932A	T	T	Y C:15.9%
5763G	ORF1a: C1833F	nsp3: C1015F	G	G	K T:10.9%
8600G	ORF1a: V2779L	nsp4: V16L	G	G	S C:12.8%
12054T	ORF1a: C3931fs	nsp7: C72fs	T	T	del 10.3%
12467G	ORF1a: A4068T	nsp8: A126T	G	G	R A:10.8%
12708C	ORF1a: A4148V	nsp9: A8V	C	C	Y T:10.1%
14460T	ORF1b: F331L	nsp12: F340L	T	T	K G:22.3%
18352T	ORF1b: L1629del, P1630del	nsp14: L105del, P106del	T	T	del 13.4%
18353T			T	T	del 13.4%
18354A			A	A	del 13.4%
18355C			C	C	del 13.4%
18356C			C	C	del 13.4%
18357T			T	T	del 13.4%
18786T	Silent	nsp14	T	T	Y C:10.3%
21575C	S: L5F	S: L5F	C	C	Y T:11.4%
23766C	S: S735L	S: S735L	C	C	Y T:11.4%
25613C	ORF3a: S74F	ORF3a: S74F	C	C	Y T:13.0%
25714C	ORF3a: L108F	ORF3a: L108F	C	C	Y T:12.3%
26355T	Silent	E	T	T	Y C:13.2%
26413T	E: Y57H	E: Y57H	T	T	Y C:12.8%
28864A	Silent	N	A	A	W T:18.9%
29409C	N: T379N	N: T379N	C	C	M A:16.1%
29708C	Silent	3'UTR	C	C	Y T:11.2%
PANGO			BA.1.18	BA.2.3	BA.2.3